Journal of Hydrology 667 (2026) 134787

Contents lists available at ScienceDirect

Journal of Hydrology

journal homepage: www.elsevier.com/locate/jhydrol

Hydropedological clustering: improving the representation of low streamflows in a semi-distributed hydrological model

Fernando Gimeno [a, b, *], Mauricio Zambrano-Bigiarini [b, c], Camila Alvarez-Garreton [b], Mauricio Galleguillos [b, d, e]

[a] Doctorate Program in Natural Resources Sciences, Universidad de la Frontera, Francisco Salazar 01145, Temuco, 4811230, La Araucanía, Chile
[b] Center for Climate and Resilience Research, Universidad de Chile, Avenida General Blanco Encalada 2002, floor 4, Santiago, 8370449, Región Metropolitana de Santiago, Chile
[c] Department of Civil Engineering, Universidad de la Frontera, Francisco Salazar 01145, Temuco, 4811230, La Araucanía, Chile
[d] Faculty of Engineering and Sciences, Universidad Adolfo Ibáñez, Avenida Diagonal Las Torres 2640, Peñalolén, 7941169, Región Metropolitana de Santiago, Chile
[e] Data Observatory Foundation, ANID Technology Center No. DO210001, Avenida Eliodoro Yáñez 2990, Providencia, 7510277, Región Metropolitana de Santiago, Chile

HIGHLIGHTS

- Hydropedological clustering improved low streamflow simulations in SWAT+.
- Hydropedological clustering reduced calibration runtime by 29 %.
- SWC-hydropedological clustering shows balanced fit (r = 0.69, RMSE = 0.059).
- Clustering is more critical than soil map resolution for low streamflow simulation.

GRAPHICAL ABSTRACT

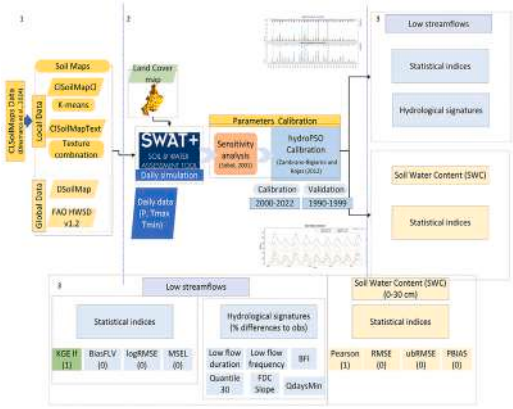

ARTICLE INFO

This manuscript was handled by Marco Borga, Editor-in-Chief, with the assistance of Kolbjorn Engeland, Associate Editor

Keywords:
Soil classification
Hydrological signatures
Soil water content

ABSTRACT

Low streamflows are critical for sustaining water supply in Mediterranean regions, yet their simulation remains challenging due to the complex influence of soils on subsurface water storage and release. This study evaluates how different soil datasets and classification approaches affect the performance of the semi-distributed, physically based SWAT+ model in simulating low streamflows and soil water content (SWC). Using the Mediterranean Cauquenes catchment in central Chile, we compared two global soil datasets (HWSDv1.2, DSOLMap) and two locally derived products (CLSoilMapsTex, CLSoilMapsCl). The latter implements a new hydropedological clustering approach based on K_s, AWC, and α. Results show that CLSoilMapsCl substantially improved low streamflow simulations (KGE_{lf} = 0.67, 44 % higher than HWSDv1.2) and reproduced hydrological signatures more accurately. These findings highlight that integrating hydropedological information enhances the representation of soil–water interactions in SWAT+, supporting more reliable low streamflow modeling and water-resource assessments in Mediterranean catchments.

* Corresponding author at: Doctorate Program in Natural Resources Sciences, Universidad de la Frontera, Francisco Salazar 01145, Temuco, 4811230, La Araucanía, Chile.
Email address: f.gimeno01@ufromail.cl (F. Gimeno).

https://doi.org/10.1016/j.jhydrol.2025.134787
Received 4 September 2025; Received in revised form 1 November 2025; Accepted 13 December 2025
Available online 19 December 2025
0022-1694/© 2025 Elsevier B.V. All rights are reserved, including those for text and data mining, AI training, and similar technologies.

1. Introduction

In Mediterranean catchments, dry-season streamflow is essential for sustaining human consumption, agriculture, energy production, and ecosystem health (Blum et al., 2019; Kirkby, 2016; Pfannerstill et al., 2014). This segment of the streamflow is referred to as low streamflows (Smakhtin, 2001; Blum et al., 2019) and typically represents the lowest 30 % of total streamflow (Pfannerstill et al., 2014; Pokhrel et al., 2012).

Soils play a central role in sustaining low streamflows by storing, transferring, and releasing water into river systems (Vereecken et al., 2014, 2019). The capacity of the soil to perform these functions depends on key hydropedological properties, such as saturated hydraulic conductivity (K_s) and available water capacity (AWC). These properties regulate subsurface flows and aquifer recharge, which provide delayed contributions to rivers during dry periods (Vanderhoof et al., 2024; Jaffrés et al., 2021; Chagas et al., 2024). Their strong spatial heterogeneity across catchments, however, makes low streamflow responses difficult to represent consistently.

Hydrological models offer a means to simulate these processes but face inherent challenges. The complexity of soil–water interactions is difficult to capture, as models require simplifying assumptions in both structure and parameterization (Cenobio-Cruz et al., 2023; Fernando et al., 2025; Muñoz-Castro et al., 2025). These models come in various architectures, ranging from simple lumped models to fully distributed systems. Choosing a specific architecture requires a certain quantity and quality of data (Fernando et al., 2025; López-Ballesteros et al., 2023). Additionally, these models demand spatially compatible data, which often proves to be a difficult task. Therefore, the selection of an adequate strategy to transform raw data into compatible model input data is crucial to ensure a robust representation of hydrological variables within a model Rivas-Tabares et al. (2020); Chen et al. (2016); Lei et al. (2024), particularly those related to low streamflows (Cenobio-Cruz et al., 2023).

Among input datasets, soils remain one of the most uncertain and influential controls on model performance (Rivas-Tabares et al., 2020; Lei et al., 2024). Coarse-resolution data often fail to capture hydrologically relevant heterogeneity, while fine-resolution data can improve representation of soil water storage and baseflow regulation (López-Ballesteros et al., 2023; Chen et al., 2016; Smit et al., 2024a). Yet, finer resolution also increases model complexity and computational demand, and does not necessarily improve overall flow simulations (Boluwade and Madramootoo, 2013; Rivas-Tabares et al., 2020). This trade-off remains poorly explored for low streamflows, despite their critical importance for water allocation during dry periods, when errors in water availability estimates have the greatest consequences.

To better assess model limitations in this context, hydrological signatures have emerged as useful diagnostic tools. These indices, derived from streamflow data, provide insights into hydrological functioning, help evaluate model performance in reproducing low streamflow dynamics, and highlight potential structural deficiencies (Richter et al., 1996; Sawicz et al., 2011; Hrachowitz et al., 2014; Westerberg and McMillan, 2015; McMillan, 2020; Addor et al., 2018).

The Soil and Water Assessment Tool (SWAT; Arnold et al., 2012) and its enhanced version, SWAT+, (Bieger et al., 2017) are semi-distributed hydrological models widely used worldwide for simulating streamflows at the catchment scale. These models simulate complex hydrological processes based on mass and energy conservation laws, relying on multiple parameters to describe the hydrological system. They can simulate not only streamflow but also sediment and nutrient transport, as well as water fluxes within the soil-plant-atmosphere system (Arnold et al., 2012) and other processes such as plant growth or carbon storage (Yang and Zhang, 2016; Abitew et al., 2023). Although SWAT+ is a physically based model, it relies on an underlying hydrological conceptual model that defines the dominant flow pathways, storage, and process interactions represented through its structure (Fig. 10), which underpins the mathematical representation of catchment processes. These models have been used for a wide range of environmental and hydrological applications, including land-cover change, uncertainty analysis, and sediment transport (e.g., Galleguillos et al., 2021; Gimeno et al., 2022; Van Tol et al., 2021; Lei et al., 2024).

In particular, SWAT+ has recently been utilized for simulating low streamflows and soil water content (SWC) (Van Tol et al., 2021; Lei et al., 2024). Despite its advanced modeling capabilities, SWAT+ often struggles to accurately simulate low streamflows, which limits our understanding of this critical hydrological process (Tegegne et al., 2019; Lei et al., 2024; Pfannerstill et al., 2014). These uncertainties hinder an accurate simulation of the water balance at the catchment scale, especially during periods of low flows, which could be particularly relevant for a precise assessment of changes in water resources (Galleguillos et al., 2021).

To simulate streamflow, SWAT+ requires diverse input datasets, among which soil properties are particularly critical. In SWAT+, soil properties must be provided as a structured and classified set of soil parameters. The model does not directly use gridded datasets of soil properties; instead, it assigns them to discrete Hydrologic Response Units (HRUs) based on categorical classifications defined by the unique combination of land cover, soil, and slope within a sub-catchment, treated as a hydrologically homogeneous unit for simulation. Therefore, even if high-resolution gridded soil products are globally available (e.g., SoilGrids; Poggio et al., 2021), their continuous property values must first be grouped or classified into discrete soil classes to meet the requirements of the model (Harrison et al., 2022; Chagas et al., 2024).

The manner in which soil information is classified and integrated into SWAT+ is crucial, as it directly determines how soil processes are represented in the simulations. Inaccurate spatial distribution or oversimplification of soil properties is a common source of model limitations, often resulting in poor representation of hydrological functions (Rivas-Tabares et al., 2020; Van Tol et al., 2021; Harrison et al., 2022). Various approaches have been developed to address these problems, including automatic classification (Rivas-Tabares et al., 2020; Liu et al., 2024), layer-specific texture-based classification (López-Ballesteros et al., 2023), and hydropedological mapping techniques (Van Tol et al., 2021; Smit et al., 2024a,b). The latter, where soils are grouped according to their hydrological behavior and properties, is particularly promising for improving the simulation of key processes in SWAT+, such as soil water storage and lateral water fluxes (Bouma, 2014; Van Tol et al., 2013, 2021; Harrison et al., 2022; Smit et al., 2024a).

To improve the simulation of low streamflows and SWC in SWAT+, in this study we explore the following two research questions:

a) Does the use of locally derived soil classifications improve SWAT+ simulations of low streamflows and SWC dynamics compared to classifications based on global datasets?
b) Between texture-based and hydropedological-based clustering, which approach provides superior performance in simulating low streamflows and soil moisture dynamics in SWAT+?

To address these objectives, we evaluate three primary soil datasets in SWAT+: i) the coarse-resolution, globally available HWSDv1.2 (Fischer et al., 2008); ii) the high-resolution, globally available DSOLMap (López-Ballesteros et al., 2023); and iii) the locally developed CLSoilMaps (Dinamarca et al., 2023). Because CLSoilMaps is a gridded dataset not initially designed for SWAT+, we applied two classification approaches to adapt it for model use. The first is the texture-based clustering method proposed by López-Ballesteros et al. (2023), which groups soils based on combinations of USDA textural classes across the first three soil layers (hereafter referred to as `CLSoilMapsTex`). The second is a newly developed hydropedological clustering approach, which utilizes k-means to group soils based on K_s, AWC, and the α parameter from the van Genuchten model (hereafter `CLSoilMapsCl`). In total, four soil datasets—two global and two local—are implemented in SWAT+

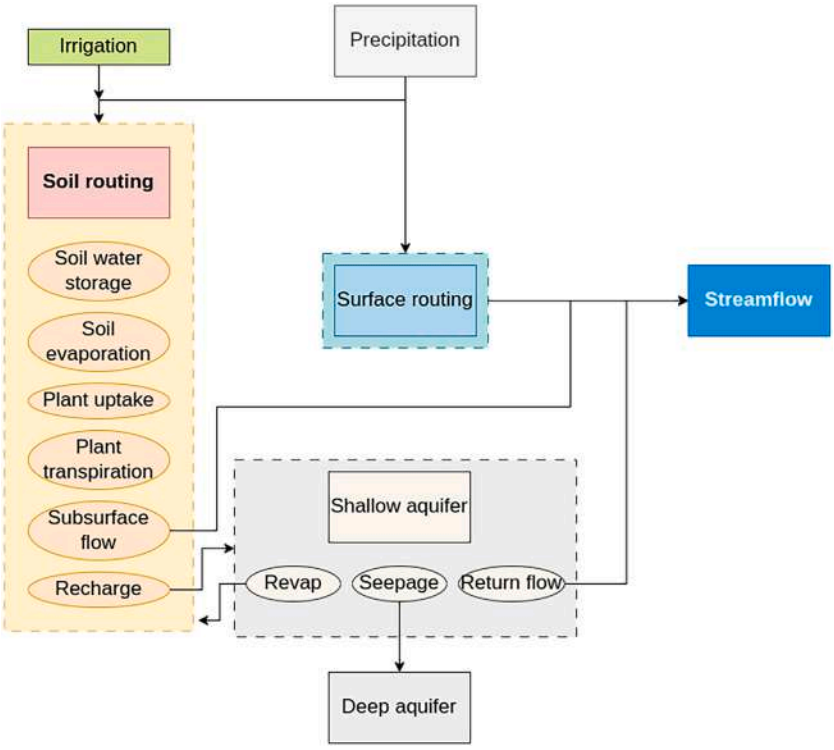

Fig. 1. Scheme of the conceptual model implicit in SWAT+, modified from (Neitsch et al., 2011).

for the same catchment and model setup, enabling a comparative assessment of their ability to simulate low streamflows and soil moisture dynamics using hydrological signatures and statistical metrics (Fig. 1).

2. Methodology

2.1. Study area

Our study area is the Cauquenes en Desembocadura River Basin, located in central Chile (Fig. 2). This catchment spans parts of the coastal mountain range and the Central Depression, and its boundaries were defined based on the location of the gauging station Río Cauquenes en Desembocadura (ID: 7339001, 35.900 °S, 72.050 °W). The total contributing area is 1750 km^2, with elevations ranging from 108 to 736 m a.s.l., a mean slope of 88.9 m km^{-1}, and a mean annual precipitation of 934 mm, concentrated mainly between April and October. Land cover is dominated by forests (41.5 %), primarily exotic plantations, and shrublands (39 %).

The climate is classified as warm-summer Mediterranean (Csb) (Rubel and Kottek, 2010), characterized by warm summers and an extended dry season that receives less than 40 mm of precipitation. During this period, low streamflows play a critical role in sustaining agricultural activities and ecosystems within the basin (Galleguillos et al., 2021).

Soils in the catchment are derived from granitic and metamorphic formations of the Chilean Coastal Mountain Range (CIREN, 1997; CIREN0, 1999). More than 20 soil classes have been identified (CIREN, 1997; CIREN0, 1999), with the predominant taxonomic orders being Alfisols, Inceptisols, and Vertisols. These soils are mostly associated with sandy-loam textures (Soto et al., 2019).

2.2. Data sources

2.2.1. Hydro-meteorological data

Daily precipitation (P) and air temperature data were obtained from 5-km resolution gridded product CR2Met (Boisier, 2023), provided by the Center for Climate and Resilience Research (CR2). This dataset covers continental Chile at a regular 0.05° latitude-longitude grid and spans the period from 1960 to the present. The temperature and precipitation rasters are based on statistical models calibrated against quality-controlled observational records. This product has been successfully validated for the study area using data from local weather stations (Galleguillos et al., 2021). Daily streamflows were obtained from the gauging station Río Cauquenes en Desembocadura, located at the catchment's outlet.

2.2.2. DEM and land cover

For the identification of the stream network and the definition of HRUs and subcatchments, we utilized a DEM derived from Light Detection and Ranging (LiDAR). The original 5 m resolution dataset derived from unmanned aerial systems (UAS) survey data, as described by Fassnacht et al. (2021). The dataset was resampled to a spatial resolution of 20 m to facilitate its integration into the hydrological model. Gaps in LiDAR coverage were filled using ALOS-PALSAR elevation data (JAXA, 2007), providing a continuous elevation surface.

For land cover, we used the CLDynamicLandCover dataset (Galleguillos et al., 2024), a dynamic land cover product developed specifically for central Chile, covering latitudes from 31.61° to 43.50°S with a spatial resolution of 30 m. This dataset provides land cover maps at five-year intervals from 1990 to 2018, and was generated using a semi-automatic classification algorithm initially developed for the coastal zone of south–central Chile (Galleguillos et al., 2024). CLDynamicLandCover uses a supervised classification approach, based on satellite data (Landsat and SRTM) representing reflectance and topographic variables, complemented by auxiliary cartographic information. The classification was trained using 15 land cover classes, photo-interpreted and georeferenced samples from 2018, to derive spectral signatures for each class. The predictor variables were selected using a combination of machine-learning algorithms and expert-driven criteria. Land cover trajectories were corrected using ecological transition rules and economic cost constraints, including reclassification adjustments for harvested plantations with overall classification accuracy ranging

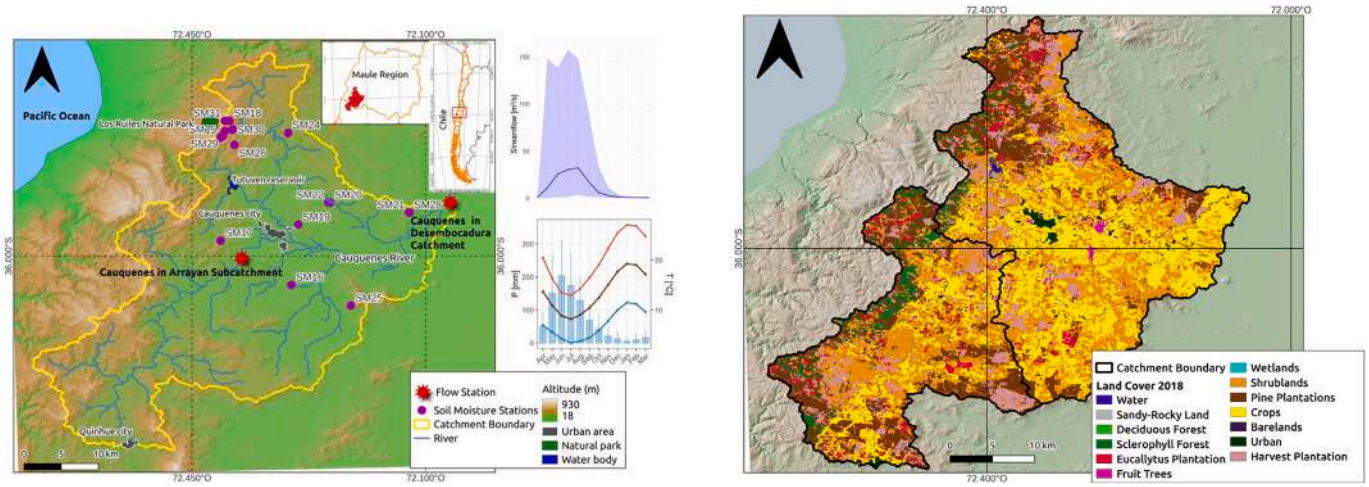

Fig. 2. (Left) Overview Río Cauquenes en Desembocadura catchment. (Right) Land cover of Cauquenes catchment during 2018 (Galleguillos et al., 2024).

Table 1
Description of local soil dataset and global soil datasets.

N	Product	Resolution	Layers N	Description
1	HWSDv1.2	1000 m	2 (0–30; 30–100 cm)	Compiled by FAO and IIASA in 2012, the Harmonized World Soil Database (HWSD) is a 30 arc-second raster with 15,000 different soil units derived from the combination of regional and national soil information with the FAO-UNESCO Soil Map of the World (FAO, 1971–1981).
2	DSOLMap	250 m	6 (0–5; 5–15; 15–30; 30–60; 60–100; 100–200 cm)	OpenLandMap is a global soil map derived from machine learning techniques and global soil profile observations (López-Ballesteros et al., 2023).
3	CLSoilMaps	100 m	6 (0–5; 5–15; 15–30; 30–60; 60–100; 100–200 cm)	CLSoilMaps is a gridded database of soil properties based on digital soil mapping (DSM) techniques and pedo-transfer functions (Rosetta V3), with a 100 m resolution covering continental Chile and binational basins shared with Argentina. It follows the GlobalSoilMap depth standard (Dinamarca et al., 2023).

from 0.894 to 0.950 and Kappa coefficients between 0.877 and 0.943 (Galleguillos et al., 2024).

2.2.3. Soil datasets

To assess the effect of using global versus local soil datasets as input data in SWAT+ for the simulation of low streamflows and SWC, we used two global datasets: i) HWSDv1.2 (Fischer et al., 2008); ii) DSOLMap (López-Ballesteros et al., 2023), and one local gridded product, CLSoilMaps (Dinamarca et al., 2023).

Table 1 summarizes the key characteristics of the soil data products used in this study.

Harmonized world soil database (HWSDv1.2)

The Harmonized World Soil Database (HWSDv1.2), developed by the FAO (Fischer et al., 2008), is a global dataset providing harmonized soil taxonomy and attributes at a spatial resolution of 30-arc-seconds (~1 km). It integrates data from multiple regional and national soil information systems, such as SOTER, ESD, WISE, and the Soil Map of China, as well as the FAO–UNESCO Soil Map of the World at 1:5,000,000 scale (FAO, 1971–1981). The database includes over 16,000 distinct soil mapping units (or soil classes) across a global grid of 21,600 rows by 43,200 columns. Each grid cell is linked to standardized attribute tables that describe key soil properties for two soil layers (0–30 and 30–100 cm), including organic carbon, pH, cation-exchange capacity, AWC, soil depth, clay content, texture class, salinity, sodium-exchange percentage, lime and gypsum content, and total exchangeable nutrients. For SWAT+ applications, this dataset was adapted by López-Ballesteros et al. (2023), who estimated additional soil-hydraulic parameters using pedotransfer functions. These estimates were necessary to derive the full set of soil input parameters required by SWAT+.

Digital soil OpenLand map (DSOLMap)

The Digital Soil OpenLand Map (DSOLMap) (López-Ballesteros et al., 2023) is a global soil dataset developed to facilitate hydrological simulations in SWAT+, integrating gridded soil information. DSOLMap is based on SoilGrids (Poggio et al., 2021), a global soil database developed by ISRIC that uses machine-learning with 350,000 soil-profile observations to generate predictions of physical and chemical soil properties across six standardized depth intervals (up to 2 m) at a 250-m spatial resolution (Poggio et al., 2021).

To adapt this gridded dataset for SWAT+ applications, WaterITech and UCAM developed an automated Python framework that processes SoilGrids map layers, first to create soil classes based on the combined

USDA textural classification of pixels for each soil layer and to extract essential SWAT+ parameters, such as soil texture, bulk density (BD), organic carbon content, and water content at field capacity and wilting point (López-Ballesteros et al., 2023). Additional properties, such as K_s, soil albedo and soil erodibility, were derived using ensembles of pedotransfer functions, following methods from Abbaspor et al. (2019). The final product, DSOLMap, is a soil database designed for global hydrological modeling and compatible with SWAT+.

CLSoilMaps

As a local soil dataset, we used CLSoilMaps (Dinamarca et al., 2023; Galleguillos et al., 2024), which is a gridded product of soil physical and hydraulic properties, developed using digital soil mapping techniques and Rosetta V3 pedotransfer functions (Schaap et al., 2001). The dataset has a spatial resolution of approximately 100 m and covers continental Chile, including transboundary basins shared with Argentina. It includes six standardized soil depth intervals, following the specifications of the GlobalSoilMap project (Arrouays et al., 2018). This gridded product is based on a newly compiled national soil profile database (Seguel et al., 2023), which integrates information from various land cover types, including agricultural lands, forests, wetlands, shrublands, and Andean grasslands. Environmental covariates were derived from SCORPAN soil-forming factors (i.e., soil, climate, organisms, relief, parent material, age, and spatial position).

2.2.4. In situ soil data

Soil water content. We included observed volumetric soil water content (SWC) data from 16 monitoring stations distributed throughout the Cauquenes catchment (Fig. 2). These stations are equipped with EnviroSCAN instruments and TEROS 10 and TEROS 12 sensors, connected to data loggers and installed at varying depths since 2018. SWC was recorded hourly and then averaged to obtain daily values. These data were used to compare simulated and observed SWC, aiming to assess how different soil datasets affect the representation of internal catchment processes in SWAT+, particularly how water is retained within the soil profile (Van Tol et al., 2021). This comparison is crucial for a deeper understanding of how different soil datasets capture the variability of low streamflows among different soil classes (Van Tol et al., 2021; Harrison et al., 2022; Smit et al., 2024a).

Soil properties. To assess the accuracy and representativeness of the soil datasets described in Section 2.2.3, we used soil-pit data from the ChSPD database as a reference (Seguel et al., 2024), a national soil-profile dataset for continental Chile. It contains 19,769 georeferenced records representing 14,029 soil profiles, with measurements of 20 physical, hydraulic, and chemical soil properties. The number of observations per property varies with the soil horizons sampled. For the Cauquenes catchment specifically, the database includes 101 soil pits. In particular, we compared texture percentages and key soil hydrological properties, such as AWC, K_s, and BD.

2.3. New soil datasets for SWAT+

SWAT+ requires grouping soil information to define Hydrologic Response Units (HRUs). Since CLSoilMaps is a gridded product, it cannot be used directly in SWAT+, because the model does not operate on a cell-by-cell basis. Therefore, the rasterized soil data must first be classified or simplified into discrete soil units to match the conceptual structure of the model. To achieve this, we applied two classification approaches to the gridded data. First, we adopted the method used to develop the DSOLMap dataset (López-Ballesteros et al., 2023), and named the resulting dataset `CLSoilMapsTex`. Second, we propose a novel hydropedological classification method that accounts for three key soil parameters controlling soil-water transfer and named the resulting dataset `CLSoilMapsCl`.

2.3.1. CLSoilMapsTex

To evaluate the influence of the soil classification methodology on hydrological simulations of low streamflows and SWC, we first implemented the method proposed by López-Ballesteros et al. (2023), which involves assigning USDA soil texture classes to each of the first three soil layers within the gridded dataset. These texture classes are then combined across the vertical profile to define unique composite soil units based on their three-layer textural configuration.

For example, if a CLSoilMaps grid cell is classified as loam in the first layer (0–30 cm), clay loam in the second layer (30–60 cm), and silty clay in the third layer (60–100 cm), its final composite class would be "loam-clay loam-silty clay". All grid cells with this exact sequence are grouped into the same soil category for hydrologic modeling purposes. This enables the preservation of vertical textural variability while simplifying the map into a manageable number of distinct soil classes.

2.3.2. CLSoilMapsCl

Second, we introduce a novel hydropedological clustering method for classifying soils based on three key hydraulic soil properties: K_s, AWC, and the α parameter from the van Genuchten model (Van Genuchten et al., 1991), all derived from the CLSoilMaps dataset. These variables were selected due to their critical role in the hydrological behavior of soils, particularly related to water transmission and retention processes (Lei et al., 2024). K_s represents the soil's ability to transfer water when it is fully saturated, strongly influencing infiltration, recharge, and subsurface flows. AWC denotes the volume of water that a soil can store and make available for plant uptake, defined as the difference between field capacity and wilting point. α describes the inverse of the air-entry suction relationship and is related to the pore-size distribution, affecting how quickly SWC changes with pressure, and therefore how responsive the soil is to drying or wetting events.

The proposed methodology is based on the widely used k-means algorithm, chosen for its simplicity and its ability to facilitate the visualization of complex multidimensional soil datasets through spatial maps during exploratory analyses (Rivera et al., 2015). Moreover, k-means has been widely applied in soil mapping and proven robust for grouping soils with similar physical or hydrological characteristics in diverse landscapes (Hot and Popovic-Bugarin, 2016; Zeraatpisheh et al., 2019; Hassan Hayatu et al., 2020).

The first step in this classification involves identifying the optimal number of clusters to represent the hydrological soil units. To achieve this, we used the ClusGap method (Tibshirani et al., 2001), which generates candidate cluster solutions with k-means and then evaluates them by comparing the observed within-cluster dispersion against that expected under a null reference distribution. The optimal number of clusters, denoted k^*, corresponds to the value of k that maximizes the gap statistic $\mathrm{Gap}(k)$ adjusted for sampling variability:

$$k^* = \arg\max_k \{\mathrm{Gap}(k) - s_{k+1}\} \tag{1}$$

where s_{k+1} is a standard deviation measure of the gap statistic.

After identifying the optimal number of clusters using the ClusGap method, the soil dataset is classified using the k-means clustering algorithm to delineate hydrological soil units. K-means divides the dataset into k clusters by minimizing the within-cluster sum of squares (WCSS), defined as:

$$\mathrm{WCSS} = \sum_{i=1}^{k} \sum_{x \in C_i} \|x - \mu_i\|^2 \tag{2}$$

where C_i is the i-th cluster, x is a data point in C_i and μ_i is the centroid of C_i.

To apply the k-means algorithm to raster data, we implemented a custom R function that incorporates spatial weights based on the `rasterkmeans` function from the R package `ecbtools` (Williamson, 2016).

In addition to soil classification maps, SWAT+ requires a soil database that specifies multiple parameters for each hydrological soil unit, including soil texture, K_s, AWC, BD, soil layer thickness, and total soil depth. For the two soil products derived from the gridded CLSoilMaps dataset (CLSoilMapsTex and CLSoilMapsCl), these parameters were directly extracted and summarized according to their respective classes. Additional variables, such as soil albedo and erodibility, were estimated using pedotransfer functions, following the methodology of Abbaspor et al. (2019). The resulting two datasets are compiled as `CLSoilSWAT` and are publicly available in Gimeno et al. (2024).

2.4. Hydrological modeling with SWAT+

2.4.1. Model description

To simulate low streamflows and SWC, we used the Soil and Water Assessment Tool Plus (SWAT+) (Bieger et al., 2017) hydrological model. This is a process-based, semi-distributed hydrological model for catchment-scale applications. It uses Hydrologic Response Units (HRUs) to represent water, sediment, and nutrient fluxes within a catchment. SWAT+ is the updated version of the original Soil and Water Assessment Tool (SWAT; Arnold et al., 2012), incorporating enhanced spatial representation and greater modeling flexibility (Bieger et al., 2017).

Hydrologic Response Units (HRUs) in SWAT+ are homogeneous spatial units in terms of soil class, land cover, slope, and water management practices (Neitsch et al., 2005). This structure enables a detailed assessment of the water balance components under varying land cover conditions (Arnold et al., 2012). In this study, surface runoff was estimated using the modified SCS Curve Number method (CN). Water movement through the leading drainage network was simulated using the variable storage routing method. Actual evapotranspiration (ETa) was calculated using the Hargreaves equation (Hargreaves and Samani, 1985), with minimum and maximum temperatures from the CR2METv2.5 dataset (Boisier, 2023). Model input data were processed using QGIS for spatial data preparation (Dile et al., 2015), and simulations were carried out using SWAT+ revision 60.5.4.

Soil water content in SWAT+

Fig. 3 shows the main processes influencing SWC simulated in SWAT+, including infiltration, soil water retention, recharge, subsurface flow, groundwater re-evaporation (referred to as Revap in SWAT+), bypass flow, evapotranspiration, and overland flow. These processes are directly or indirectly influenced by the soil properties provided as parameters in the soil datasets.

In any given day, the simulation of SWC in SWAT+ is driven by the following water balance equation (all the terms are in mm H_2O):

$$SW_t = SW_0 + \sum_{i=1}^{t} \left(R_{\text{day}} - Q_{\text{surf}} - E_a - w_{\text{seep}} - Q_{\text{gw}} \right) \quad (3)$$

where SW_t is the final SWC, SW_0 is the initial soil water content on day i, t represents the time in days, R_{day} is the precipitation, Q_{surf} accounts for the surface runoff, E_a denotes the actual evapotranspiration, w_{seep} represents the water entering the vadose zone from the soil profile, and Q_{gw} is the groundwater return streamflow.

For more details on the SWAT+ soil water balance structure and governing equations, refer to Neitsch et al. (2011) and Appendix A.

2.4.2. SWAT+ implementation

Once the individual soil maps for the Cauquenes catchment were available, they were independently integrated into the SWAT+ model, keeping all other inputs constant. The four SWAT+ models used to simulate streamflow and SWC were therefore named HWSDv1.2, DSOLMap, CLSoilMapsCl, and CLSoilMapsTex, reflecting the soil dataset on which each model was based.

When these different soil datasets were introduced into SWAT+ for the Cauquenes catchment, distinct configurations of Hydrologic Response Units (HRUs) emerged due to variations in soil classification and spatial resolution. The CLSoilMapsTex dataset yielded the highest number of HRUs (1296), reflecting the increased heterogeneity of the map, whereas CLSoilMapsCl generated 903 HRUs. In contrast, the global datasets HWSDv1.2 and DSOLMap produced 783 and 1208 HRUs, respectively.

We evaluated whether the differences among the simulations using different soil datasets were statistically significant. We first tested the normality of model outputs using the Kolmogorov-Smirnov test. Given the non-normal distributions in all cases, pairwise comparisons were conducted using the Wilcoxon test from the stats R package (Bauer, 1972; R Core Team, 2025) where the differences were significant ($p - value < 0.001$).

2.4.3. Model calibration

To reduce the number of parameters to be calibrated, a sensitivity analysis was performed on 20 parameters, selected based on various literature sources. The sensitivity analysis was carried out using a variance-based global sensitivity analysis technique (Sobol) (Saltelli et al., 2010), which provides an efficient and robust approach to assess parameter sensitivity across their full range of values. The parameters included in the analysis are listed in Table 3, and their physical ranges were obtained from the SWAT+ user manual (Bieger et al., 2017) (Table 2).

Once the sensitive parameters were obtained, the four models were calibrated using the global optimization algorithm hydroPSO (Zambrano-Bigiarini et al., 2013), with the objective function defined as the modified Kling-Gupta Efficiency (KGE) for low streamflows (Garcia et al., 2017) (Eq. 4), which utilizes the KGE by Gupta et al. (2009) (KGE 2009).

$$KGE_{lf} = \frac{\text{KGE}(Q) + \text{KGE}(1/Q)}{2} \quad (4)$$

where KGE_{lf} is the Kling-Gupta Efficiency for low streamflows, calculated as the average of the standard KGE (Gupta et al., 2009) applied to the observed and simulated streamflow (Q) and to the inverse of streamflow ($1/Q$).

The hydroPSO calibration uses the default particle swarm optimization (PSO) algorithm, as described by Zambrano-Bigiarini et al. (2013). The initial parameter values were set to the default values provided by SWAT+. The parameter ranges for calibration were taken from the SWAT+ user manual (Bieger et al., 2017).

The simulation was divided into three phases: a warm-up (1989), a calibration phase (2000–2022), and a validation phase (1990–1999). This structure prioritized model calibration for a more recent period, including the 2010–2022 mega-drought (Garreaud et al., 2025), thereby enhancing the model's ability to simulate prolonged low streamflow conditions.

2.4.4. Evaluation of low streamflows

Following calibration, we evaluated the daily streamflow simulations by comparing them against observations from the Cauquenes gauging station at Desembocadura. As the primary objective of this study was to assess the performance of low streamflow simulation, we focused the evaluation on this streamflow segment using a set of commonly applied statistical indices. We included the log-transformed Root Mean Square Error ($logRMSE$) (Bekele and Nicklow, 2007) to emphasize low-flow accuracy during calibration (Pfannerstill et al., 2014). Additionally, we used the Bias for Low Flow Volume ($BFLV$) and the Mean Square Error of Log Discharge ($MSEL$), both proposed by Pokhrel et al. (2012). $MSEL$ is particularly effective in capturing model performance during periods of hydrograph recession.

$$\text{logRMSE} = \sqrt{\frac{1}{N} \sum_{i=1}^{N} \left(\log \left(\frac{\tilde{Q}_i}{Q_i} \right) \right)^2} \quad (5)$$

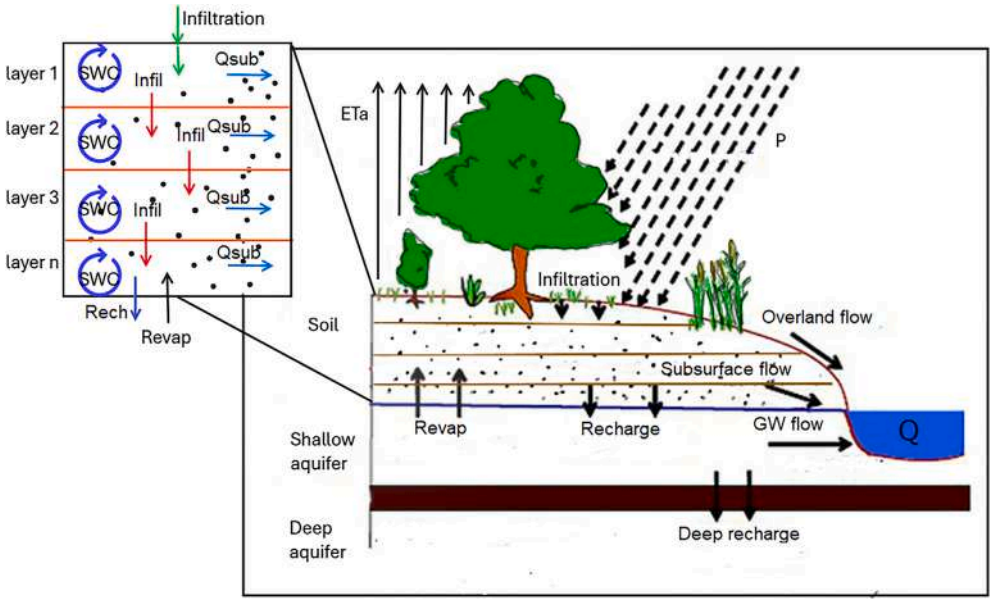

Fig. 3. Water movement in SWAT+, with a focus on soil water dynamics within the model. Modified from Arnold et al. (2012).

Table 2
Model parameters used in the sensitivity analysis.

N	Parameter	Archive	Default value	Range	Description
1	ALPHA_BF	aquifer.aqu	0.05	0–1	Alpha factor for groundwater recession curve (1/day)
2	REVAP	aquifer.aqu	0.02	0.02–0.2	Groundwater revap coefficient
3	PERCO	hydrology.hyd	0.5	0–1	Recharge coefficient
4	CN	cntable.lum	–	0.8–1.2	Curve Number
5	FLOW_MIN	aquifer.aqu	3	0–10	Threshold depth from surface to water table for groundwater flow to occur (m)
6	REVAP_MIN	aquifer.aqu	5	0–10	Threshold depth from surface to water table for revap to occur (m)
7	LATQ_CO	hydrology.hyd	0.01	0–1	Lateral flow coefficient
8	Soil_K	soil.sol	–	0.01–10	Soil saturated hydraulic conductivity (K_s)
9	Soil_AWC	soil.sol	–	0.8–1.2	Available Water Capacity (AWC)
10	Soil_BD	soil.sol	–	0.8–1.2	Soil bulk density (BD)
11	Soil_CBN	soil.sol	–	0.5–1.5	Soil Carbon
12	SPEC_YLD	aquifer.aqu	0	0–0.4	Specific yield of the aquifer
13	ESCO	hydrology.hyd	0.5	0.01–1	Soil evaporation compensation factor
14	EPCO	hydrology.hyd	0	0.01–1	Plant uptake compensation factor
15	RCHG_DP	aquifer.aqu	0	0–1	Recharge coefficient from shallow to deep aquifer
16	CAN_MAX	hydrology.hyd	1	0–100	Maximum canopy storage (mm)
17	CAN_HT_MAX	plant	–	0.75–1.25	Maximum canopy height
18	RT_DP_MAX	plant	–	0.8–1.2	Maximum root depth
19	CN3_SWF	hru.rlt	1	0–1	Soil water factor for CN3
20	gw_flo	aquifer.aqu	0.05	0–2	Initial groundwater flow

where N is the total number of time steps, $\tilde{Q}$ and Q are the simulated and observed discharges at time step i, respectively. The term $\log\left(\frac{\tilde{Q}}{Q}\right)$ reduces the influence of extreme values by emphasizing relative deviations.

$$\text{BiasFLV} = \frac{\sum_{i=1}^{N}\left(\tilde{Q}_{\text{low},i} - Q_{\text{low},i}\right) \times 100}{\sum_{i=1}^{N} Q_{\text{low},i}} \tag{6}$$

where $\tilde{Q}_{\text{low}}$ and Q_{low} are the simulated and observed low streamflows at time step i, respectively.

$$\text{MSEL} = \frac{1}{N}\sum_{i=1}^{N}\left(\log_{10}(\tilde{Q}_i) - \log_{10}(Q_i)\right)^2 \tag{7}$$

where $\tilde{Q}$ and Q are the simulated and observed streamflow at time step i, respectively. The logarithmic transformation reduces the influence of high flows and emphasizes model performance during recessions.

Additionally, we conducted a visual inspection of the Flow Duration Curve (FDC) for each model, focusing on their respective low streamflow segments. The FDC shows the percentage of time that a given streamflow is equaled or exceeded, effectively representing the flow probability distribution (Kincheon S., 1959). For diagnostic purposes, it is essential to identify specific discharge ranges where the model underperforms. We examined FDC segments for low (Q70–Q95), and very low flows (Q95–Q100). The exceedance probability ranges from 0 % to 100 %, with Q100 representing the discharge that is exceeded 100 % of the time.

FDC has been widely used to evaluate streamflow simulation performance, particularly for assessing high-flow events, typically associated with exceedance probabilities below 2 % (Yilmaz et al., 2008). In contrast, the low streamflow segment is typically evaluated within an exceedance range of 70 % to 100 %, where discharges with exceedance probabilities between 70 % and 95 % are classified as low streamflows, and those exceeding 95 % are classified as very low streamflows (Pfannerstill et al., 2014).

In our study, we incorporated hydrological signatures to assess specific aspects of catchment hydrological behavior for the low streamflow segment and to evaluate the model's ability to reproduce these

Table 3
Summary of hydrological signatures. A more detailed description is given in Appendix B.

Hydrological signature	Description	Reference	Equation
low_Q_dur	**Low Flow Duration**. Continuous period during which daily streamflow is less than 20 % of the mean discharge	(Addor et al., 2018)	$low\_Q\_dur = \frac{1}{N}\sum_{i=1}^{N} D_i$ (8)
low_Q_frec	**Low Flow Frequency**. Average number of daily low streamflow events per year yr^{-1}, defined using a threshold of 20 % of the mean daily streamflow.	(Addor et al., 2018)	$low\_Q\_frec = \frac{N}{T}$ (9)
BFI	**Baseflow Index**. Ratio of baseflow to total streamflow over a given period	(McMillan, 2020)	$BFI = \sum_{i=1}^{N} \frac{Q_i \mathrm{b}}{Q_i}$ (10)
QuantileN	Streamflow value corresponding to the 70th percentile of the flow duration curve	(Addor et al., 2018)	
QnDaysMin	**Low Flow Magnitude**. Mean streamflow during the seven consecutive days with the lowest flows in the time series	(Richter et al., 1996)	$QnDaysMin = \frac{1}{7}\sum_{i=1}^{7} Q_{\min,i}$ (11)
FDC_slope	Slope of the flow duration curve, typically calculated between the 33rd and 66th percentiles. In this study, the 70th and 95th percentiles were computed to characterize the low streamflow segment.	(Sawicz et al., 2011)	$FDC\_slope = \frac{\ln(Q_{70\,\%}) - \ln(Q_{95\,\%})}{0.95 - 0.70}$ (12)

dynamics across different soil data configurations. These signatures capture key hydrological processes—such as low streamflow duration, low streamflow frequency, or baseflow, providing a valuable complement to standard statistical metrics (McMillan, 2020; Pizarro and Jorquera, 2024). We employed a set of hydrological signatures (Table 3) to evaluate variations in low streamflow dynamics.

2.4.5. Simulation of soil water content

The soil water content (SWC) simulated by SWAT+ was evaluated against in situ observations to assess the model's ability to represent soil moisture dynamics under different soil datasets (Vereecken et al., 2019; Vanderhoof et al., 2024). In SWAT+, SWC is reported for each soil layer as the amount of water stored within the available water capacity (AWC), expressed in millimeters of water. For this study, we used the output corresponding to the upper 30 cm layer and, additionally, computed the root-zone (0–100 cm) SWC as the cumulative average across layers.

To compare with field measurements, the simulated SWC (mm) was converted to volumetric soil water content ($m^3\ m^{-3}$) using the soil layer thickness (Δz, mm) as follows:

$$SWC_{vol} = \frac{SWC_{mm}}{\Delta z} \tag{13}$$

Observed SWC values were measured at different depths across the monitoring network. To harmonize these measurements with the simulated depths, we estimated the representative SWC at 30 cm and 100 cm (root-zone) using the depth-weighted approach of Li et al. (2005):

$$SWC = \left(0.10 \times \theta_1 + 0.90 \times \theta_2\right) \tag{14}$$

where SWC represents the SWC ($m^3\ m^{-3}$) in the upper 30 cm of the soil, and θ denotes the fractional SWC in layer i, in this example considering two layers.

Additionally, simulated soil water content (SWC) in SWAT+ is reported as the amount of water stored within the available water capacity (AWC) of each soil layer, expressed in millimeters of water. Because the model does not calculate the permanent wilting point (PWP) internally, the AWC values provided as input already represent the difference between field capacity and PWP. To facilitate comparison with in situ soil moisture data (reported in volumetric units and representing the total SWC), we estimated PWP externally following the equation provided in the SWAT theoretical manual and Zare et al. (2022), (Eq. 15).

$$WP_{ly} = 0.4 \cdot \frac{m_c \times \rho_b}{100} \tag{15}$$

where WP_{ly} is the water content at the wilting point, m_c is the percent clay content of the layer (%), and ρ_b is the BD for the soil layer ($g\ cm^{-3}$).

This correction allowed expressing simulated SWC in volumetric units consistent with the observed data and ensured a comparable reference for model evaluation. Comparisons between simulated and observed SWC were conducted daily. Simulated values were extracted from the water balance output of the corresponding Hydrologic Response Unit (HRU), where each SWC monitoring station was located. Model performance was evaluated at the surface depth, with a particular emphasis on capturing the temporal dynamics of SWC. For this purpose, we used the Pearson correlation coefficient to assess temporal agreement, the Root Mean Square Error (RMSE) to quantify deviations between simulated and observed values, the Percent Bias (PBIAS) to measure the model's tendency to over- or underestimate observations, and the unbiased Root Mean Square Error (ubRMSE) to quantify the random errors after bias removal, reflecting the model's ability to capture temporal variability (Entekhabi et al., 2010).

2.5. Workflow

Fig. 4 illustrates the integration of advanced soil mapping and hydrological modeling using SWAT+ to simulate daily hydrological processes and assess the dynamics of the catchment. Inputs include soil maps (CLSoilMaps clusters, CLSoilMaps textures, DSOLMap, and FAO HWSDv1.2), land cover maps, and hourly/daily climate data (P, max temperature Tmax, and min temperature Tmin). The process incorporates parameter sensitivity analysis (Sobol, 2001) and calibration using Particle Swarm Optimization (PSO) for the calibration (2000–2022) and validation (1990–1999) periods. The first step (panel 1) involves creating the SWAT+ input using local soil data. In the second step (panel 2),

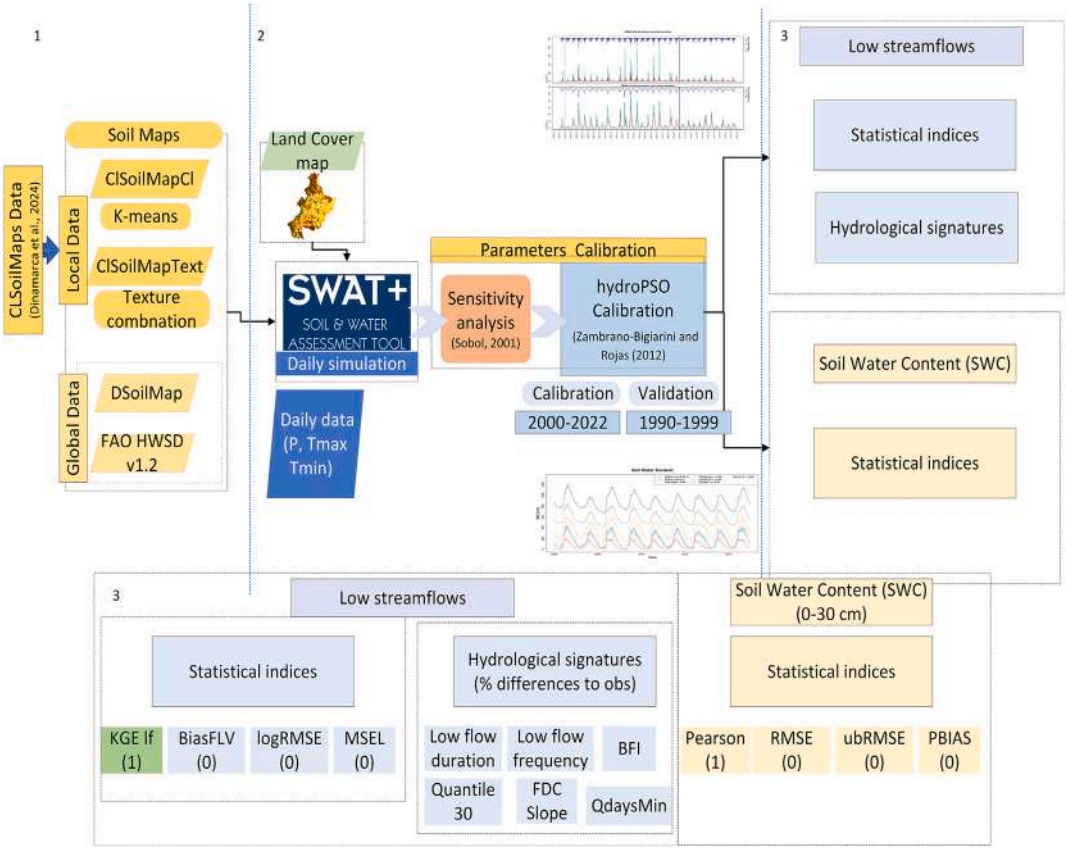

Fig. 4. Research workflow, divided into three main steps. 1) Soil Maps as Input for SWAT+. 2) SWAT+ runs with sensitivity analysis and calibration. 3) Results analysis with statistical and hydrological signatures metrics.

the SWAT+ model is run, and the most sensitive parameters are calibrated. The third step (panel 3) focuses on analyzing low streamflows and SWC simulations.

3. Results

3.1. New soil datasets

Based on the CLSoilMaps gridded dataset, we developed two new high-resolution soil datasets for continental Chile, specifically tailored for SWAT+ modeling applications.

The first new soil dataset, CLSoilMapsTex, resulted in 53 soil classes within the Cauquenes catchment while maintaining the six-layer structure and standardized depth intervals defined in CLSoilMaps. For each hydrological soil unit, CLSoilMapsTex provides per-layer values for SWAT+ parameters, including AWC, K_s, BD, texture fractions, soil albedo, and the soil erodibility index.

For the k-means classification based on key hydropedological properties (AWC, K_s, and α), the ClusGap statistic, identified six optimal soil clusters in the Cauquenes catchment. Accordingly, the CLSoilMapsCl dataset was generated with these six soil classes, preserving the six-layer depth structure of CLSoilMaps and providing the same suite of SWAT+ parameters as CLSoilMapsTex.

In contrast, the global datasets HWSDv1.2 and DSOLMap represent the Cauquenes catchment with only three and 32 soil classes, respectively, while maintaining their original layer configurations and parameter values from the source products (Fig. 5).

Fig. 6 compares soil texture and hydropedological properties across five datasets: Observations from 101 soil pits in the Cauquenes catchment, CLSoilMapsCl, CLSoilMapsTex, DSOLMap, and HWSDv1.2. The top-left bar plot displays that CLSoilMapsCl has the highest sand content, while HWSDv1.2 exhibits the highest clay content. The AWC boxplot indicates that observed soils exhibit greater variability and higher median water retention, while HWSDv1.2 and DSOLMap consistently underestimate AWC. In the K_s plots, the observed values show a wide distribution, while HWSDv1.2 and DSOLMap display low and narrow ranges, suggesting limited infiltration estimates. Lastly, the BD boxplot reveals that observed data spans the broadest density range, with HWSDv1.2 and DSOLMap producing more constrained and higher values.

3.2. SWAT+ calibration

In the sensitivity analysis focused on low streamflows, the most influential parameter was FLO_MIN (Appendix C), which represents the threshold depth from the surface to the water table for groundwater flow to occur. K_s (called SOL_K in SWAT+) was also sensitive (Appendix C). Other soil-related parameters, such as PERCO (which governs the rate of infiltration between layers) and the lateral flow coefficient (LATQ_CO), are also functionally tied to soil hydraulic behavior and are sensitive. For instance, when K_s values are low, PERCO tends to compensate by allowing more vertical movement. Similarly, lateral flow is inherently controlled by both soil texture and conductivity, demonstrating the indirect but important influence of soil properties on model sensitivity. These sensitive parameters are not only important for streamflow simulations, but also for SWC.

Based on the Sobol sensitivity analysis using CLSoilMapsCl, we retained the 11 most influential and identifiable parameters for calibration across all soil-map scenarios. To isolate the effect of the soil datasets themselves, we fixed soil saturated hydraulic conductivity (K_s) to the values provided by each map and excluded K_s from calibration. Calibrating K_s would have retuned the very property that differs most between maps, introducing compensation and masking true

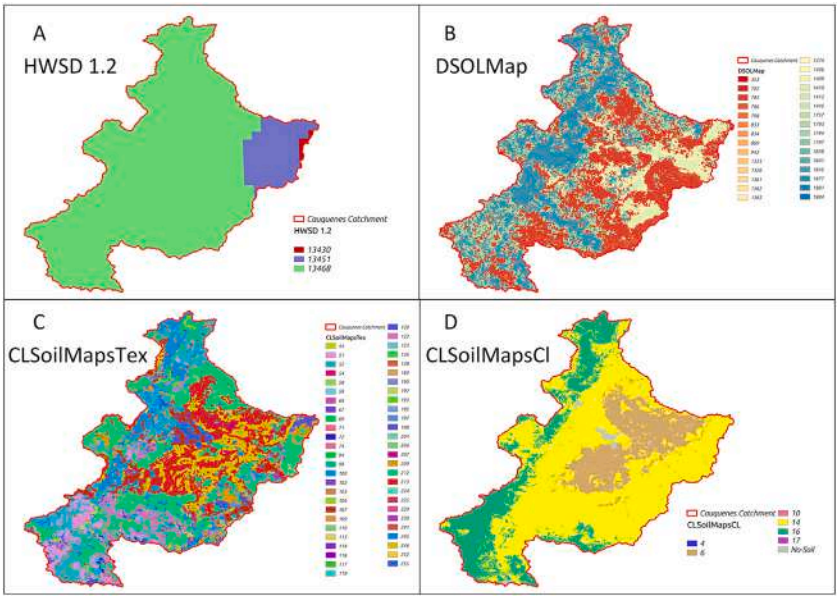

Fig. 5. Soil classification maps in the cauquenes catchment: A) HWSDv1.2 from FAO (Fischer et al., 2008); B) DSOLMap (López-Ballesteros et al., 2023); C) CLSoilMapsTex grouped by textural class combinations; D) CLSoilMapsCl grouped by k-means.

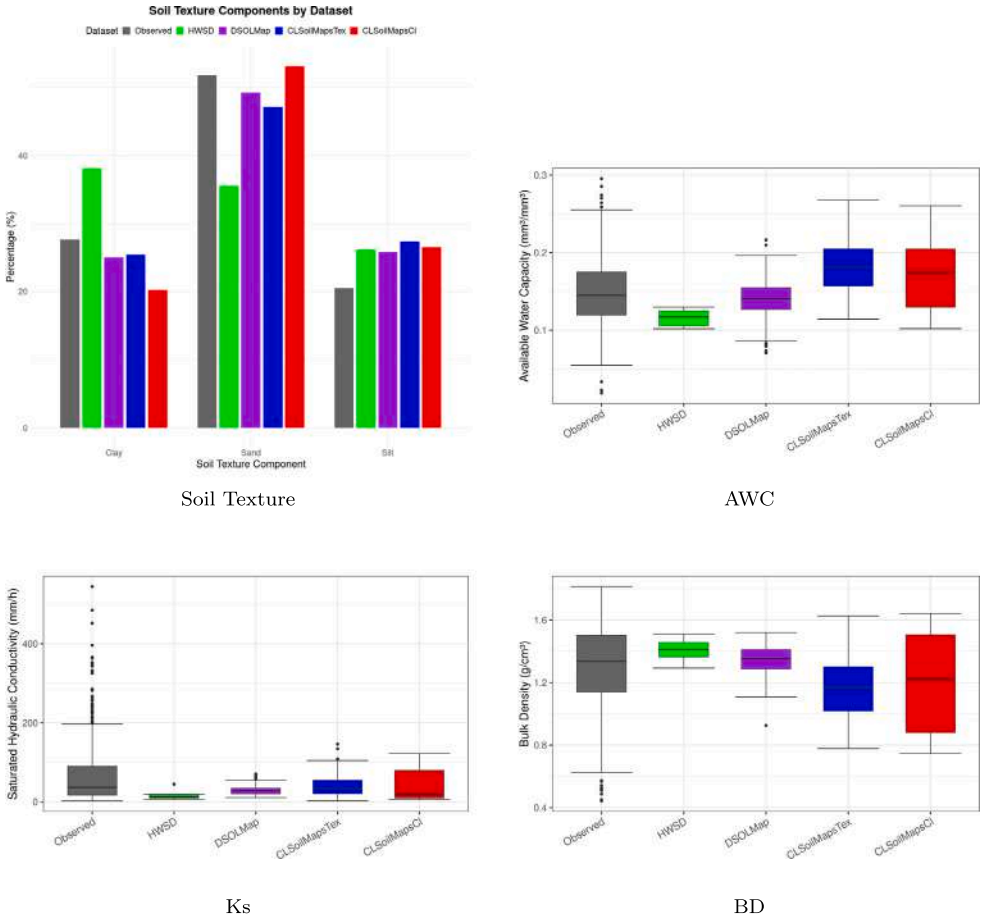

Fig. 6. Comparison of soil texture and hydraulic properties (AWC, K_s, BD) across five datasets: field observations, HWSDv1.2, DSOLMap, CLSoilMapsTex, and CLSoilMapsCl.

dataset-driven contrasts in SWC and runoff partitioning (i.e., confounding the treatment effect). We included CN2 in the final calibration set because allowing limited adjustment of surface runoff potential helps prevent structural bias from propagating into groundwater and evapotranspiration parameters (e.g., ALPHA_BF, RCHRG_DP, ESCO, REVAP). This design preserves between-map hydraulic contrasts (via

Table 4
List of parameters retained for calibration after Sobol sensitivity analysis and their configurations.

N	Parameter	Archive	Method	Default value	Calibration range	Description
1	FLOW_MIN	aquifer.aqu	Replace	3	0–10	Threshold depth from surface to water table for groundwater flow to occur (m)
2	REVAP	aquifer.aqu	Replace	0.02	0.02–0.2	Groundwater revap coefficient
3	RCHG_DP	aquifer.aqu	Replace	0	0–1	Recharge coefficient from shallow to deep aquifer
4	PERCO	hydrology.hyd	Replace	0.5	0–1.	Recharge coefficient
5	REVAP_MIN	aquifer.aqu	Replace	5	0–10	Threshold depth from surface to water table for revap to occur (m)
6	LATQ_CO	hydrology.hyd	Replace	0.01	0–1	Lateral flow coefficient
7	SPEC_YLD	aquifer.aqu	Replace	0	0–0.4	Specific yield of the aquifer
8	CN3_SWF	hru.rlt	Replace	1	0–1	Soil water factor for CN3
9	ESCO	hydrology.hyd	Replace	0.5	0.01–1	Soil evaporation compensation factor
10	ALPHA_BF	aquifer.aqu	Replace	0.05	0–1	Alpha factor for groundwater recession curve (1/day)
11	CN2	cntable.lum	Mult	–	0.8–1.2 multiplication	Curve Number

fixed K_s) while maintaining model fidelity through the most influential, non-redundant parameters.

The calibrated values, along with those of the remaining parameters, were obtained using the hydroPSO algorithm and are presented in Appendix D, and Table 4 presents the complete list of calibrated parameters.

Under the same calibration parameters and computational configuration, total calibration times were approximately 12 h for CLSoilMapsCl, 17 h for CLSoilMapsTex, 12 h for HWSDv1.2, and 16 h for DSOLMap. These simulations were executed on a high-performance Linux server (Ubuntu, kernel 5.15.0) equipped with dual Intel® Xeon® Gold 6438 M processors (64-cores, 128-threads, 2.6 GHz) and 256 GB RAM.

3.3. Simulation of low streamflows

For low streamflows, the daily results for the calibration period (2010–2022) and validation period (1990–2010) are presented in Fig. 7. All the models were evaluated using several metrics of performance: Kling-Gupta efficiency for low streamflows (KGE_{lf}) (Garcia et al., 2017), log root mean square error (logRMSE) (Bekele and Nicklow, 2007), mean squared error in log space (MSEL) (Pokhrel et al., 2012), and bias in low streamflow volume (BiasFLV) (Pokhrel et al., 2012).

During calibration, CLSoilMapsCl exhibited the highest KGE_{lf} (0.63), indicating a better agreement with the observed low streamflow dynamics compared to other models. However, it also presented the highest BiasFLV (13.56 %) with an overestimation of low streamflow volumes. DSOLMap and CLSoilMapsTex showed relatively balanced performance with BiasFLV values of 9.48 % and 8.07 %, respectively, and KGE_{lf} values above 0.56. In contrast, HWSDv1.2 showed the lowest KGE_{lf} (0.49), indicating greater difficulties in capturing low streamflow variability. When considering logRMSE, CLSoilMapsCl exhibited the lowest error (1.14), while CLSoilMapsTex and HWSDv1.2 showed higher values of 1.33 and 1.31, respectively. These results suggest that soil maps incorporating local data (CLSoilMapsCl, CLSoilMapsTex) outperform the HWSDv1.2 dataset in simulating low streamflow conditions.

During validation, CLSoilMapsCl maintained the best performance in terms of KGE_{lf} (0.67) and logRMSE (0.89), confirming the robustness of locally derived soil maps in reproducing low streamflow dynamics. However, its BiasFLV persisted at a high level (31.15 %), indicating continued overestimation of low flows. CLSoilMapsTex showed a decrease in KGE_{lf} (0.46), but maintained stable MSEL (0.27), indicating moderate reliability in different periods.

The HWSDv1.2 model showed the poorest performance during the validation period, with the lowest KGE_{lf} (0.45), and a BiasFLV of −23.42 %, indicating a severe underestimation of low streamflow conditions. The DSOLMap model demonstrated improved performance during validation, with a BiasFLV of −0.04 %.

We also analyzed low streamflow events during dry years (1990–1991), as shown in Fig. 8. This figure compares the low streamflows observed and simulated for four modeling approaches: a) HWSDv1.2, b) DSOLMap, c) CLSoilMapsTex, and d) CLSoilMapsCl. CLSoilMapsCl demonstrates the best agreement with observed flows, with a KGE_{lf} of 0.6, an MSEL of 0.01, and a BiasFLV of −14.21 %, suggesting a moderate underestimation of low flows. In contrast, CLSoilMapsTex exhibits an overestimation, reflected in a BiasFLV (164.45 %), a higher logRMSE (0.95) and MSEL (0.17). The HWSDv1.2 shows the weakest performance, with a low KGE_{lf} (0.05), a higher MSEL (0.06), and a BiasFLV (68.44 %), highlighting the deviations from observed conditions. Meanwhile, DSOLMap also exhibits low performance, with a KGE_{lf} of −2.09, an MSEL of 0.12, and BiasFLV of 88.61 %, highlighting substantial overestimation of low streamflows. Overall, CLSoilMapsCl provides the best performance simulation of low streamflows, whereas DSOLMap and CLSoilMapsTex exhibit larger discrepancies.

The Flow Duration Curves (FDCs) for low streamflows (Q70–Q95 range of the probability of exceedance) provide a detailed comparison of observed and simulated results from different models. Panel A in Fig. 9, illustrates the observed FDC, capturing the overall streamflow characteristics and emphasizing the low streamflow regime. The CLSoilMapsCl (panel B, red) performs moderately well, with an FDC slope of 7.81 compared to the observed value of 8.92, indicating a reasonable representation of low streamflows. However, it shows some deviations in the upper part of the exceedance probability range (Q70–Q80). In contrast, the CLSoilMapsTex (panel C, blue) exhibits discrepancies compared to the observed curve line with overestimation below 80 % exceedance probability and underestimation above this threshold, but its FDC slope (8.6) remains close to the observed value. The HWSDv1.2 scenario (panel D, green) demonstrates poor visual performance, with an FDC slope of 10.49. However, the DSOLMap scenario (panel E, purple) overestimates low streamflows with an FDC slope of 17.93.

Table 5 compares the hydrological signatures at the catchment outlet between the observed and simulated values using different soil datasets. The observed Low Flow Duration was 16.5 days, and the CLSoilMapsCl dataset produced the closest result (13.2 days), while CLSoilMapsTex strongly underestimated it (7.8 days). The global datasets produced intermediate values, with 11.4 days for HWSDv1.2 and 9.2 days for DSOLMap. In terms of Low Flow Frequency, all models showed a good agreement with the observed frequency of 0.26. CLSoilMapsCl reproduced it almost exactly (0.27), and DSOLMap provided the lowest estimate (0.23).

The Baseflow Index (BFI), which quantifies the contribution of baseflow to total streamflow, was most poorly represented by CLSoilMapsTex (0.53), substantially exceeding the observed value of 0.36. The global datasets HWSDv1.2 and DSOLMap produced more moderate overestimations (0.41 and 0.39, respectively), while CLSoilMapsCl showed the best agreement (0.34). For the 30th percentile flow (Q30), the observed value was 0.75 m/s. All simulations overestimated these values, with CLSoilMapsTex again performing worst (1.95 m/s) and CLSoilMapsCl performing best (0.84 m/s).

The minimum flow for N days (QnDaysMin), an indicator of drought intensity, was best reproduced by CLSoilMapsCl (0.24 m/s) compared

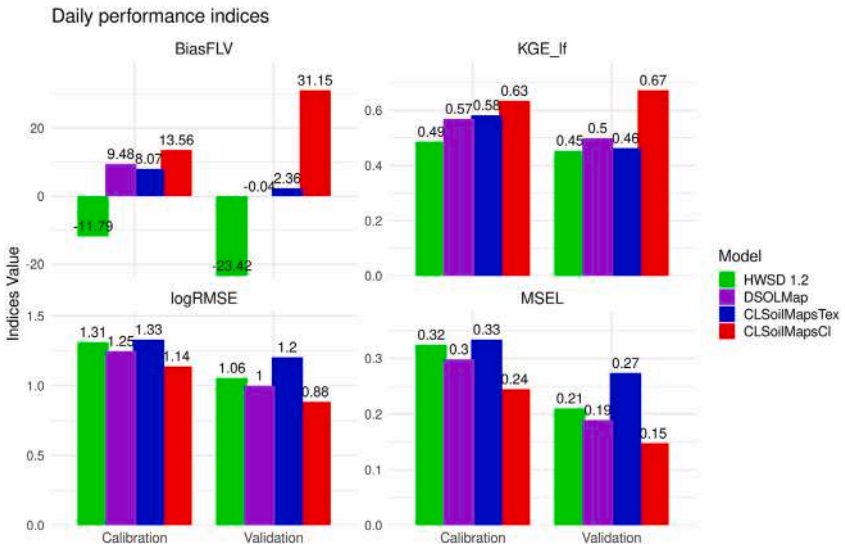

Fig. 7. The figure illustrates the performance of the different models during the calibration (2000–2022) and validation (1990–1999) periods.

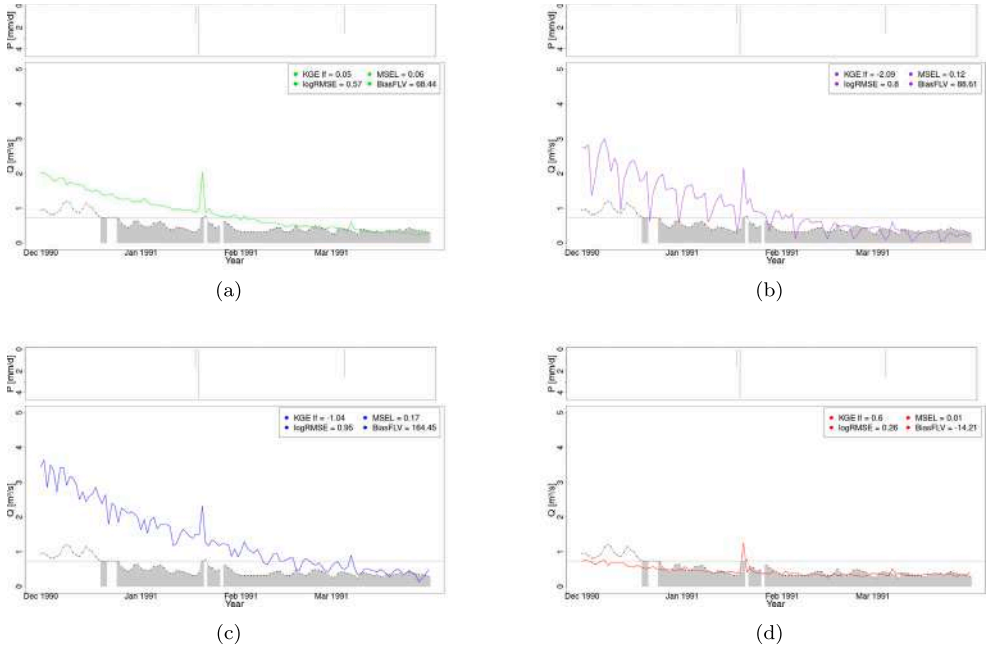

Fig. 8. Comparison of observed and simulated low streamflow conditions for different soils maps for the hydrologic year 1990–1991. Each sub-figure represents a different simulation method: a) HWSDv1.2, b) DSOLMap, c) CLSoilMapsTex, and d) CLSoilMapsCl. The gray-shaded region indicates the range of observed low streamflow bands, while the colored shaded region represents the simulated low streamflows within the observed band. Key performance metrics include KGE_{lf}, logRMSE, MSEL, TRMSE, and BiasFLV.

to the observed 0.17 m/s, whereas CLSoilMapsTex, HWSDv1.2, and DSOLMap substantially underestimated this metric (0.08, 0.07, and 0.02 m^3/s, respectively). The slope of the flow duration curve (FDC slope) exhibited considerable variability. The observed value was 8.92, with CLSoilMapsCl (7.81) and CLSoilMapsTex (8.60) providing the closest approximations. In contrast, DSOLMap vastly overestimated the slope (17.93), indicating a much sharper transition between high and low flows.

For the relative differences with respect to the observed hydrological signatures, (Fig. 10), CLSoilMapsCl (red line) showed the closest overall alignment with observations, maintaining the lowest relative differences across all metrics. HWSDv1.2 (green line) also performed well, especially in QnDaysMin and Quantile 30, although it showed more variability in other metrics. DSOLMap (purple line) had some discrepancies, with higher deviations in FDC slope and Low Flow Frequency. In contrast, CLSoilMapsTex (blue line) showed the largest deviation from observed values, particularly in Baseflow Index, Q30, and Low Flow Frequency, indicating a poorer representation of hydrological behavior. Overall, this figure suggests that CLSoilMapsCl provides the most consistent performance in replicating observed hydrological signatures, while CLSoilMapsTex tends to overestimate or misrepresent several critical flow characteristics. The global datasets, although they perform better than CLSoilMapsTex, present overestimations relative to the observed hydrological signatures.

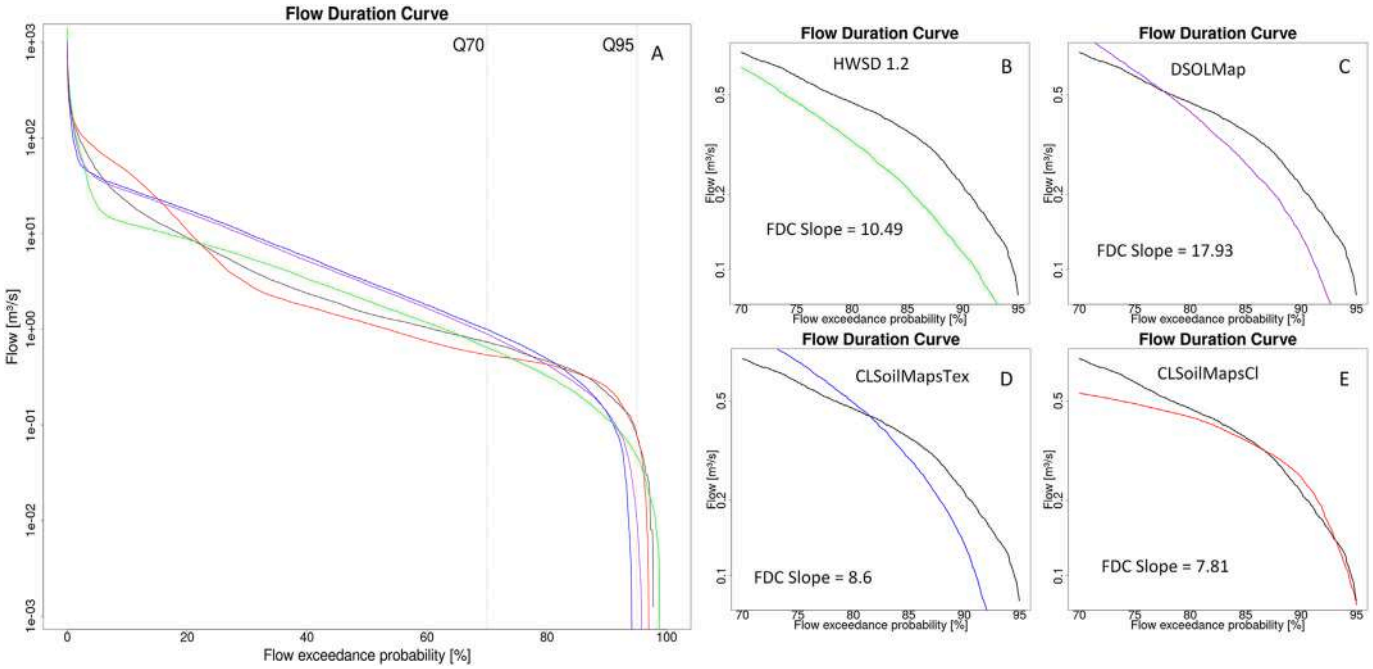

Fig. 9. Flow duration curves (FDCs) for low flows (Q70–Q95). Panel A shows observed FDCs, while Panels B–E compare observed and simulated low-flow regimes for different models. FDC slope is included as a performance metric.

Table 5
Hydrological signatures for Cauquenes gauging station and for the different simulations.

Signatures	Obs	HWSDv1.2	DSOLMap	CLSoilMapsTex	CLSoilMapsCl
Low streamflow duration (days)	16.5	11.4	9.2	7.8	13.2
Low streamflow frequency	0.26	0.21	0.23	0.20	0.27
Baseflow index	0.36	0.41	0.39	0.53	0.34
Quantile 30 (m^3/s)	0.75	0.93	1.47	1.95	0.84
QnDaysMin (m^3/s)	0.17	0.07	0.02	0.08	0.24
FDC slope	8.92	10.49	17.93	8.60	7.81

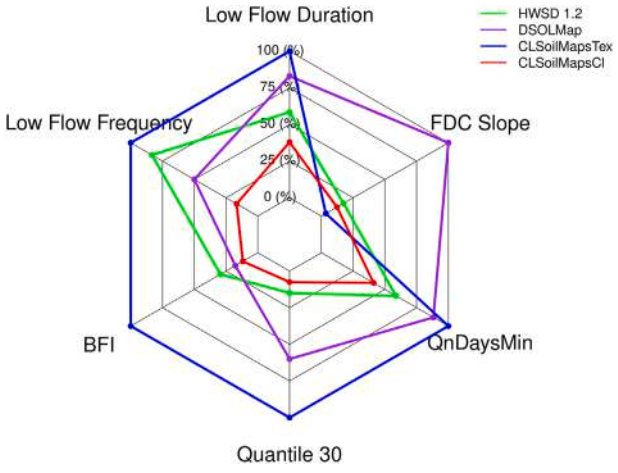

Fig. 10. The figure shows the relative deviation of four simulations, HWSDv1.2 (green line), DSOLMap (purple line), CLSoilMapsTex (blue line), and CLSoilMapsCl (red line), from observed hydrological signatures across six metrics: Low Flow Duration, Low Flow Frequency, Baseflow Index (BFI), Quantile 30, QnDaysMin, and FDC slope. In this plot, 0 % indicates perfect agreement with observations (good performance), while 100 % represents the greatest relative differences among the datasets (low performance).

3.4. Evaluation of soil water content

The distribution of surface SWC (30 cm) over the months revealed seasonal variability (Fig. 11). Observed data (gray) showed changes throughout the year, with increases during winter (wet period), as expected. Model simulations exhibited less variability throughout the year and were unable to reproduce the seasonal differences between wet and dry periods.

To complement the surface analysis, we also evaluated the soil water content in the root zone (0–100 cm) (Fig. 12). We observed a similar seasonal behavior to surface SWC, but with overestimation, especially in the winter season.

Table 6 summarizes the performance of the four soil datasets (CLSoilMapsCl, CLSoilMapsTex, HWSDv1.2, and DSOLMap) in simulating soil water content (SWC) at both the surface (0–30 cm) and root-zone (0–100 cm) layers. At the surface, `HWSDv1.2` exhibited the highest correlation (R^2 = 0.76) but also the largest RMSE (0.166 m^3 m^{-3}), indicating strong temporal agreement but large absolute errors. In contrast, `CLSoilMapsCl` achieved a balanced performance with relatively high correlation (R^2 = 0.69) and low RMSE (0.059 m^3 m^{-3}). `DSOLMap` showed the lowest RMSE (0.055 m^3 m^{-3}) but a moderate correlation (R^2 = 0.63), suggesting minimal deviations despite weaker temporal consistency. For the unbiased RMSE (ubRMSE), `DSOLMap` and `CLSoilMapsCl` yielded comparable values (0.054 and 0.054 m^3 m^{-3}), confirming their superior

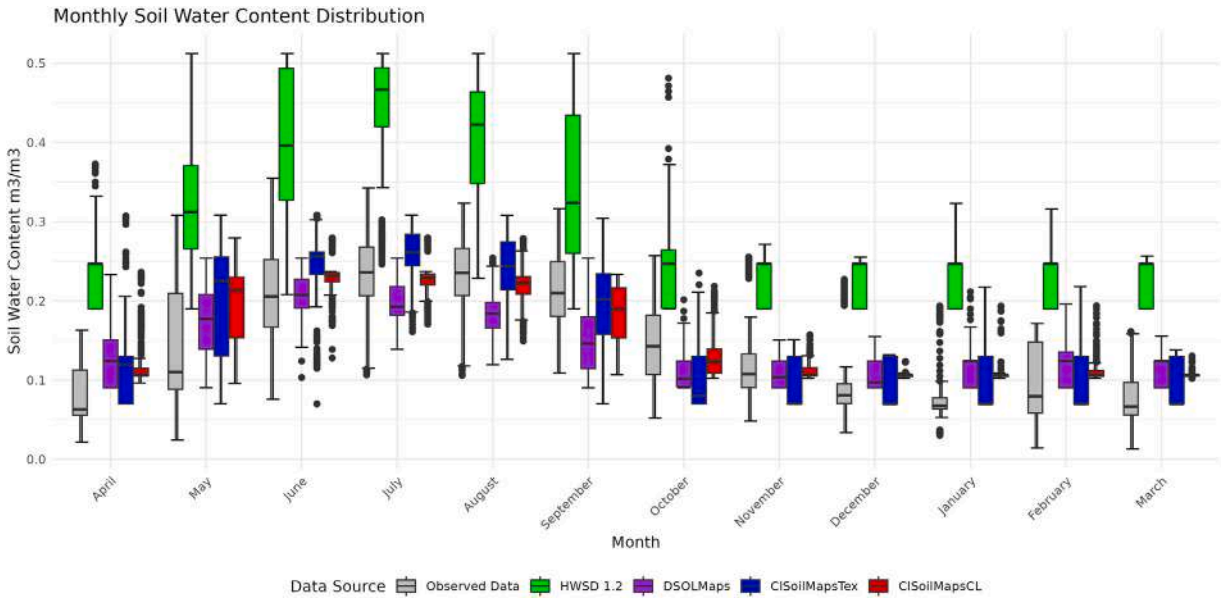

Fig. 11. Dynamic simulations of soil water content at 30 cm.

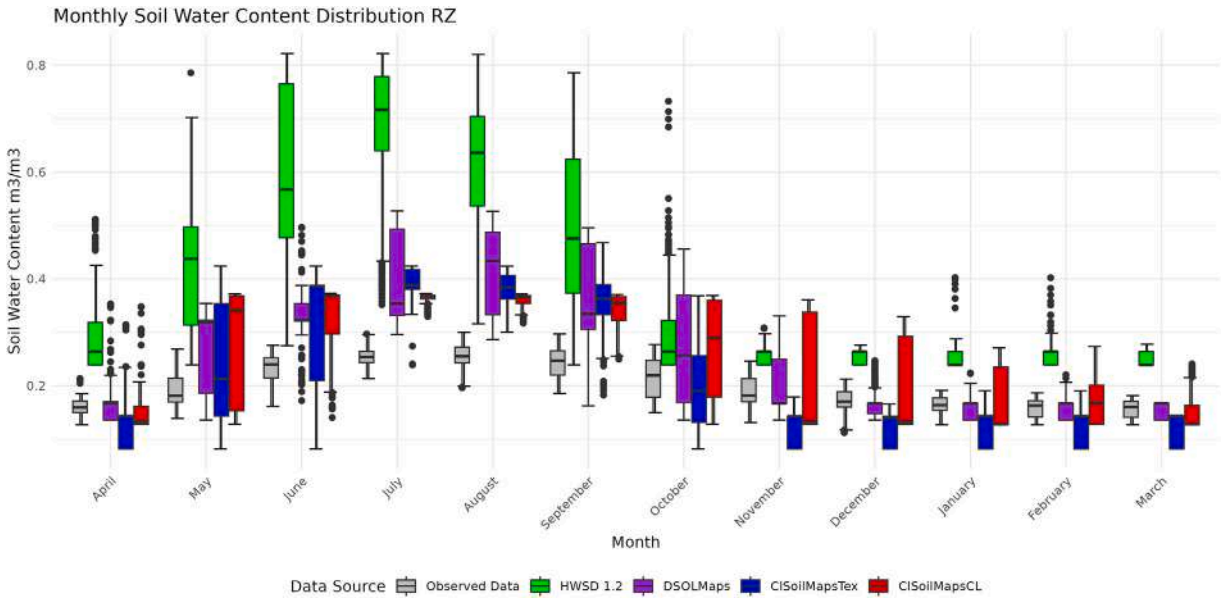

Fig. 12. Dynamic simulations of soil water content at root-zone (0–100 cm).

Table 6
Performance of soil water content (SWC) simulations for surface (0–30 cm) and root-zone (0–100 cm) layers.

Depth	Soil dataset	Correlation (R^2)	RMSE (m^3/m^3)	ubRMSE (m^3/m^3)	PBIAS (%)
Surface (0–30 cm)	HWSDv1.2	0.76	0.166	0.0642	103.9
	DSOLMap	0.63	0.055	0.0544	−1.1
	CLSoilMapsTex	0.61	0.071	0.0692	7.6
	CLSoilMapsCl	0.69	0.059	0.0538	9.3
Root-zone (0–100 cm)	HWSDv1.2	0.60	0.285	0.1340	175.5
	DSOLMap	0.72	0.135	0.0648	82.7
	CLSoilMapsTex	0.57	0.116	0.0848	55.0
	CLSoilMapsCl	0.72	0.126	0.0544	79.6

trade-off between accuracy and stability. `CLSoilMapsTex` presented the weakest performance (correlation = 0.61, RMSE = 0.071 m^3 m^{-3}), emphasizing that texture-based classification alone was less effective in reproducing observed surface SWC dynamics.

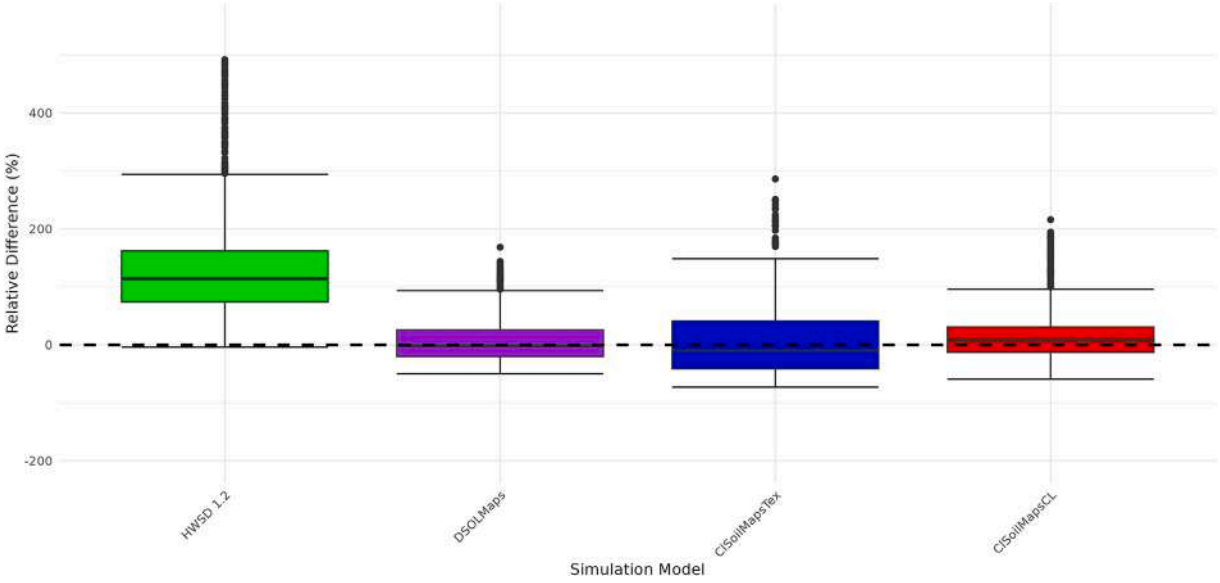

Fig. 13. Relative differences between simulated soil and observed point data for September, October, and November.

In the root zone (0–100 cm), the locally derived datasets again outperformed the global products. `CLSoilMapsCl` achieved the highest coefficient of determination (R^2 = 0.72) with an RMSE of 0.126 m^3 m^{-3} and a PBIAS of 79.6 %, while `CLSoilMapsTex` obtained a lower RMSE (0.116 m^3 m^{-3}) and PBIAS of 55.0 %. The global datasets `DSOLMap` and `HWSDv1.2` exhibited weaker agreement with observations, with RMSE values of 0.135 and 0.285 m^3 m^{-3}, respectively, and higher positive biases (82.7 % and 175.5 %).

For the four soil datasets, Fig. 13 shows the relative differences (%) for spring months (September, October, November) between the simulated and observed SWC. The CLSoilMapsCl and CLSoilMapsTex exhibited the smallest mean relative differences with observed data (17.1 % and 3.04 %, respectively). Simulations based on HWSDv1.2 had the highest mean relative difference (130 %) and a greater spread than the local dataset simulations, indicating an overestimation of SWC compared to observations. Results derived from DSOLMap had a moderate mean relative difference (7.31 %) with slightly lower variability. The dashed horizontal reference line at 0 % highlights the bias direction, with HWSDv1.2 showing a clear tendency toward overestimation. These results suggest that CLSoilMapsTex provided the most accurate simulation, while HWSDv1.2 introduced the largest discrepancy in SWC estimations. Appendix E presents daily observations and simulations of SWC.

4. Discussion

4.1. New soil data and SWAT+ implementation

In the Cauquenes catchment, global datasets such as HWSDv1.2 and DSOLMap exhibited relatively homogeneous soil property values across their classes, particularly for available water capacity (AWC), soil saturated hydraulic conductivity (K_s), and bulk density (BD). In contrast, soil properties derived from CLSoilMaps showed the highest variation of these properties among soil classes, consistent with patterns observed in field data. Notably, this occurs even when the number of classes is small; for example, CLSoilMapsCl, despite having only six soil classes, captures greater horizontal and vertical variability in AWC, K_s and BD, than DSOLMap, which includes 30 classes. This pattern supports earlier findings from Dai et al. (2019), who conducted a comprehensive review of global soil property maps and noted the challenges in representing both the spatial and vertical heterogeneity of soil properties. Similarly, Bodenstein et al. (2022) identified these limitations when comparing the spatial and profile variability of soil properties between global datasets, such as the HWSDv1.2, the SOTER dataset, and the continental product AfSoilGrids 250 m, against observed data obtained from soil profiles with two distinct layers. They found that global products often struggle to accurately capture both the horizontal and vertical variability of soil properties. Efforts to improve the accuracy of the global SoilGrids 2.0 dataset have highlighted the need to increase the number of soil observations to better capture spatial heterogeneity, particularly in high-latitude regions (Poggio et al., 2021). The prediction accuracy for soil properties, especially AWC and K_s, tends to decline with depth, reflecting weaker correlations between environmental covariates and deeper layers. Similar limitations were identified for Chile, where comparisons between SoilGrids and observed soil profiles revealed difficulties in representing spatial heterogeneity (Dinamarca et al., 2023).

We also found that grouping soil data by either hydropedological clustering (CLSoilMapsCl) or textural classification (CLSoilMapsTex) had a direct influence on the model's structure and performance. The number and structure of HRUs generated in SWAT+ varied notably across soil datasets, with CLSoilMapsTex producing 1296 HRUs compared to 903 for CLSoilMapsCl, resulting in longer calibration times (17 vs. 12 h, respectively) despite using the same hardware and model configuration. This finding aligns with previous research that a higher number of HRUs and excessively detailed input data increase model complexity (Pandey et al., 2021) and calibration instability (Yen et al., 2014).

For simulating daily streamflows, CLSoilMapsCl achieved satisfactory performance, with a KGE of 0.61 in calibration and 0.55 in validation. CLSoilMapsTex performed slightly worse during the calibration (KGE = 0.52) but improved during the validation (KGE = 0.59). These results suggest that increasing spatial detail—such as using a larger number of soil classes—does not necessarily improve model performance. For instance, Rivas-Tabares et al. (2019) improved SWAT performance (NSE from 0.61 to 0.86) by reorganizing a detailed 69-class soil map into 16 hydrologically meaningful clusters using Self-Organizing Maps (SOM), thereby enhancing the spatial representation of soil properties. Raw textural data have been found to require more extensive calibration to reach comparable results (Brighenti et al., 2019), while high-resolution datasets without hydrological structuring can increase model uncertainty (Hörmann et al., 2009). Overall, SWAT performance appears to be more sensitive to input data classification and hydrological representativeness than to spatial resolution alone (Yen et al., 2014).

4.2. Simulation of low streamflows

In agreement with previous research, we found that a good representation of soil hydropedological properties is essential for accurately capturing low streamflows. Analyses across multiple catchments in Brazil identified these properties as major controls on hydrological behavior (Chagas et al., 2024), while a PCA conducted over 750 catchments in Australia highlighted soil indices among the key catchment characteristics influencing low flows (Jaffrés et al., 2021).

This finding is also supported by the results of our sensitivity analysis, which revealed that the parameters strongly influenced by the soil dataset, such as PERCO, Flow Min coefficient, (together with soil parameters such as K_s) were among the most sensitive for simulating low streamflows. These results corroborate findings by Cordeiro et al. (2018), who identified soil water retention and transmission parameters as the most influential in water-limited catchments. In our case, a Mediterranean water-limited catchment, the dominance of infiltration and lateral flow-related parameters reinforces the importance of selecting soil maps that accurately represent these processes.

Simulations of low streamflows in SWAT+ were significantly affected by the choice of soil input data, with CLSoilMapsCl achieving superior performance while maintaining model efficiency. Among the soil datasets tested, CLSoilMapsCl, which had a KGE_{lf} of 0.67 (validation period), better matched the observed values for Low Flow Duration (13.2 days closer to the observed 16.5 days), QnDaysMin (0.24 m^3/s compared to the observed 0.17 m^3/s), and Baseflow Index (0.34, observed 0.36).

The previous results are likely related to the ability of SWAT+ implemented with CLSoilMapsCl to better capture hydropedological behavior by emphasizing key functional soil properties such as K_s and AWC (Vereecken et al., 2019; Hrachowitz et al., 2021). This includes improving water retention by considering the α value from the van Genuchten curve and AWC in the k-means clustering, as well as K_s for infiltration and lateral water flow (Vereecken et al., 2019; Smit et al., 2024a; Harrison et al., 2022). Such mechanisms have also been emphasized in earlier research. Detailed soil maps that capture hydropedological behavior, particularly lateral flows, have been shown to improve streamflow simulations, increasing KGE values from 0.6 and 0.3 (calibration and validation) with national South African soil maps to 0.8 and 0.7 when using hydropedological soil maps (Harrison et al., 2022).

Soil depth also plays a fundamental role in regulating low streamflows, as it determines both water storage capacity and the potential for subsurface flow during dry periods. The harmonized datasets used in this study (HWSDv1.2, DSOLMap, and CLSoilMaps) adopt a standardized depth of 2 m, consistent with other global products such as SoilGrids, to allow intercomparison across contrasting climatic regions and facilitate integration with large-scale hydrological and biogeochemical models. However, this assumption can be restrictive at the catchment scale, where actual depths vary considerably. Analysis of 104 local soil profiles in the Cauquenes catchment revealed that most soils are relatively deep: over 70 % of profiles exceed 1 m with the 34 % exceeding 1.6 m, and several soils surpassing 2 m. Given that these pits were manually excavated, the true depths are likely even greater. Field observations and previous studies in central Chile further indicate that root water uptake frequently extends beyond 2 m into saprolitic and weathered rock layers that store available water (Galleguillos et al., 2017). These conditions suggest that the uniform 2 m assumption is less restrictive in this basin and that local soils possess sufficient depth and storage capacity to sustain low streamflows.

Multi-objective calibration combining soil water content (SWC) and streamflow observations has also demonstrated that K_s and AWC are key variables for improving low-flow simulations (Choudhary and Athira, 2021). Further studies have highlighted the central role of K_s and soil water retention capacity in shaping low streamflow dynamics, showing that underestimating K_s reduces recharge and subsurface flow. At the same time, higher AWC helps sustain streamflows during dry periods (Lei et al., 2024; Chagas et al., 2024; Martínez-Fernández et al., 2023). Model experiments and sensitivity analyses consistently isolate these soil properties as critical determinants for simulating low streamflows.

Our results show that the hydrological relevance and structure of soil data are more critical than spatial resolution alone for modeling low streamflows. While higher-resolution datasets can improve performance (López-Ballesteros et al., 2023), several studies emphasize that hydropedological classifications provide more robust improvements. For instance, hydropedological soil maps enhanced lateral flow modeling in semi-arid South Africa (Smit et al., 2024b), and the integration of hydropedological knowledge has substantially improved streamflow simulations during arid periods (Smit et al., 2024a; Van Tol et al., 2021; Harrison et al., 2022). These findings highlight that function-guided clustering, as implemented in CLSoilMapsCl, offers an efficient and robust approach for simulating low streamflows.

4.3. Representation of SWC

Our study evaluated the performance of different soil datasets, highlighting that the local soil map based on hydrological soil properties, specifically K_s, AWC, and α, shows a good performance for SWC simulation. At 30 cm, the CLSoilMapsCl model achieved a good balance between correlation (R^2 = 0.69) and other error metrics (RMSE = 0.059 m^3/m^3, ubRMSE = 0.0538), outperforming the global DSOLMap and HWSDv1.2. In particular, HWSDv1.2 showed a higher PBIAS (103.9 %) and a higher RMSE (0.166), despite a strong correlation (0.76).

A similar pattern was observed in the root zone (0–100 cm), where `CLSoilMapsCl` and `CLSoilMapsTex` again outperformed the global datasets. `CLSoilMapsCl` achieved the highest coefficient of determination (R^2 = 0.72) with an RMSE of 0.126 $m^3\ m^{-3}$ and a PBIAS of 79.6 %, while `CLSoilMapsTex` showed a slightly lower RMSE (0.116 $m^3\ m^{-3}$) and a PBIAS of 55.0 %. In contrast, `HWSDv1.2` exhibited the largest discrepancies (RMSE = 0.285 $m^3\ m^{-3}$, PBIAS = 175.5 %), maintaining its tendency to overestimate water storage. Locally derived soil datasets more accurately represent both the magnitude and vertical distribution of soil moisture, consequently, improving the capacity of SWAT+ to simulate subsurface storage and delayed flow contributions to low streamflows.

These findings are consistent with Van Tol et al. (2021), who demonstrated that incorporating hydropedological guidance in soil classifications improves SWC simulations in SWAT+ by better representing subsurface water processes, increasing the R^2 from 0.4 to 0.49, and reducing the PBIAS from 100 % to 40 %.

Building on these results, the analysis of SWC provided additional insights into model behavior and its capacity to reproduce hydrological dynamics (Han et al., 2012; Chen et al., 2011). Previous studies have shown that explicitly incorporating SWC into multi-objective calibration improves the simulation of low streamflows in SWAT+, underscoring the strong coupling between SWC dynamics and low streamflow generation (Choudhary and Athira, 2021). In our case, the relatively low bias and correlation achieved by the clustered soil dataset (CLSoilMapsCl) suggest that hydropedological soil maps not only improve SWC simulations but also enhance the representation of processes governing seasonal variability in SWC. Nevertheless, to further refine model performance, future efforts should integrate information from the root zone SWC, which is directly linked to subsurface processes (Wang et al., 2023; He et al., 2025).

Despite these advantages, the soil water model in SWAT+ does not explicitly resolve vertical SWC profiles under unsaturated conditions (Arnold et al., 2012). Previous studies have shown that such simplifications can mask subsurface heterogeneity, especially in complex or forested landscapes (Park et al., 2014). Future improvements, such as multi-variable calibration and simulation of the SWC at different soil

layers (He et al., 2025), could enhance the representation of SWC and overall model performance. Additionally, further research should explore the potential of remote sensing data and data assimilation techniques to improve temporal dynamics and constrain uncertainty, particularly in Mediterranean catchments with a long dry season where SWC plays a critical role in seasonal water availability (Martínez-Fernández et al., 2023; González-Zamora et al., 2024).

5. Conclusion

This study highlights the impact of soil data classification on simulating low streamflows and soil water content (SWC) in SWAT+. Using the Mediterranean Cauquenes catchment as a case study, we compared simulations derived from two global soil datasets (HWSDv1.2 and DSOLMap) and two locally derived high-resolution soil maps (CLSoilMapsTex, CLSoilMapsCl). We emphasize that soil maps designed to capture soil–water interactions, following a hydropedological approach such as CLSoilMapsCl, can improve low streamflow simulations.

Our main findings are summarized as follows:

- Using local soil data, we found that hydropedological clustering (CLSoilMapsCl) substantially improved low-flow simulations. During the validation period, KGE_{lf} increased to 0.67, about 40 % higher than simulations with global datasets (HWSDv1.2 = 0.45; DSOLMap = 0.50). CLSoilMapsCl also reproduced hydrological signatures more consistently with observations, estimating a low-flow duration of 13.2 days compared to 16.5 days observed, whereas DSOLMap and HWSDv1.2 simulated shorter durations (9.2 and 11.4 days, respectively). In contrast, the local texture-based dataset (CLSoilMapsTex) did not achieve comparable improvements, underscoring the added value of a hydropedological approach.
- Hydropedological clustering also enhanced computational efficiency. Calibration runtime was reduced by approximately 29 % with CLSoilMapsCl compared to CLSoilMapsTex (12 h vs. 17 h), while maintaining strong performance. This demonstrates that incorporating hydropedological information can improve both model accuracy and efficiency in semi-distributed hydrological models such as SWAT+.
- For soil water content (SWC), simulations using CLSoilMapsCl and CLSoilMapsTex aligned more closely with observed monthly medians, particularly during spring, with deviations of 17.1 % and 3.0 %, respectively. In contrast, HWSDv1.2 largely overestimated SWC (mean relative difference 130 %). Both CLSoilMapsCl and DSOLMap provided balanced trade-offs between correlation and error minimization (R^2 = 0.69 and 0.63; RMSE = 0.059 and 0.055, respectively), while HWSDv1.2, despite its higher correlation (0.76), yielded the largest error (RMSE = 0.166). Nonetheless, across all datasets, SWAT+ underestimated seasonal variability, particularly during dry periods, pointing to persistent limitations in representing soil–water–plant interactions.
- For surface soil water content (SWC), simulations using `CLSoilMapsCl` and `CLSoilMapsTex` aligned more closely with observed monthly medians, particularly during spring, with deviations of 17.1 % and 3.0 %, respectively. In contrast, `HWSDv1.2` largely overestimated SWC (mean relative difference 130 %). Both `CLSoilMapsCl` and `DSOLMap` provided balanced trade-offs between correlation and error minimization (R^2 = 0.69 and 0.63; RMSE = 0.059 and 0.055, respectively), while `HWSDv1.2`, despite its higher correlation (0.76), yielded the largest error (RMSE = 0.166). When extended to the root zone (0–100 cm), `CLSoilMapsCl` maintained the highest agreement with observations (R^2 = 0.72; RMSE = 0.126; PBIAS = 79.6 %), outperforming global datasets that showed stronger overestimation, particularly `HWSDv1.2` (RMSE = 0.285; PBIAS = 175.5 %). These results demonstrate that locally derived hydropedological soil maps improve the vertical representation of soil moisture storage and seasonal dynamics, enhancing the simulation of subsurface processes that sustain low streamflows. Nonetheless, across all datasets, SWAT+ still underestimated the seasonal amplitude of surface SWC, especially during dry periods, and overestimated the SWC in the root zone during wet periods, underscoring the need to refine soil–water–plant interaction parameterization for water-limited environments.

Overall, our findings suggest that hydropedological clustering for soil classification in SWAT+ contributes to a more accurate representation of low streamflows and SWC dynamics in Mediterranean catchments. The superior performance of the hydropedological clustering (CLSoilMapsCl) approach in the Cauquenes catchment can be directly linked to its local field conditions, characterized by shallow, texturally diverse soils and strong spatial contrasts in hydraulic conductivity that govern subsurface storage and delayed flow contributions during the dry season. By grouping soils according to their hydrological behavior rather than solely by texture, CLSoilMapsCl captures these controls more effectively, leading to a better representation of low streamflow generation processes. Beyond this specific case, the approach provides a transferable framework for improving low streamflow simulations in other Mediterranean regions worldwide, where water scarcity and heterogeneous soil–water interactions similarly challenge model performance. Hence, hydropedological clustering offers a practical pathway to enhance process representation and model reliability under water-limited conditions.

CRediT authorship contribution statement

Fernando Gimeno: Writing – original draft, Investigation, Formal analysis, Conceptualization. **Mauricio Zambrano-Bigiarini:** Writing – original draft, Supervision, Resources, Project administration, Conceptualization. **Camila Alvarez-Garreton:** Conceptualization, Methodology, Validation. **Mauricio Galleguillos:** Writing – original draft, Supervision, Resources, Project administration, Formal analysis, Conceptualization.

Declaration of competing interest

The authors declare that they have no known competing financial interests or personal relationships that could have appeared to influence the work reported in this paper.

Acknowledgements

Agencia Nacional de Investigación y Desarrollo / Programa de Becas / Beca Doctorado Nacional ANID 21221783 (ANID Chilean scholarship). FONDECYT Regular 1212071 (The catchment's memory: understanding how hydrological extremes are modulated by antecedent soil water content conditions in a warmer climate). FONDECYT Regular 1210932 (Improving forest water yield and productivity quantification at the catchment scale by mapping root depth and eco-physiological thresholds with remote sensing and water transfer modeling). FONDECYT Regular 1250718 (Unravelling the role of hydropedological processes on water yield and tree carbon sequestration of native forest ecosystems). PCI CONICYT Chile - NSFC China NSFC190018 (Management of global change impacts on hydrological extremes by coupling remote sensing data and an interdisciplinary modeling approach). Center for Climate and Resilience Research CR2 (CONICYT/ FONDAP/1523A0002). C.A-G. was partially funded by ANID/Fondecyt Iniciación/11240924 ("The role of hydrological memory and human influence on drought propagation and recovery").

Appendix A

The **Infiltration** in the model is governed by precipitation input and initial soil water content conditions and is estimated using the SCS

Curve Number method, where infiltration declines as the soil saturates. **Soil water retention** is defined through the available water capacity (AWC), given by the user as a parameter per soil layer. The wilting point is estimated in SWAT using a pedotransfer function based on soil clay content and bulk density (BD). After that the FC is calculated:

$$WP = 0.004 \cdot \frac{c \cdot b}{100} \tag{A.1}$$

where c is the percent clay content, and b is the bulk density (g/cm^3). The field capacity is then computed as:

$$FC = WP + AWC \tag{A.2}$$

Soil water retention is determined by the available water capacity (AWC) provided per soil layer. In SWAT, the wilting point is estimated using a pedotransfer function based on soil clay content and bulk density, after which the field capacity (FC) is calculated as the sum of the wilting point and the AWC. Water movement in SWAT is categorized into saturated and unsaturated flow. Only saturated flow is simulated directly. SWAT assumes uniform moisture distribution within a soil layer, thereby excluding horizontal unsaturated flow. Vertical unsaturated processes are indirectly accounted for via root uptake and soil evaporation depth distributions.

When the soil water content exceeds the field capacity, excess water becomes available for **recharge** to deeper layers or **lateral flow** downslope. Recharge is computed using a storage routing method in which the flow depends on the excess water above the field capacity and the K_s. **Lateral flow** is modeled as the movement of saturated water within the soil layer, driven by slope gradient, K_s, drainable porosity, and slope length. A lag function is applied to the lateral flow component to account for delayed lateral response, which is especially important in large hillslopes and low streamflow simulations. Recharge is first defined as:

$$SW_{\text{ly,excess}} = SW_{\text{ly}} - FC_{\text{ly}} \quad \text{if } SW_{\text{ly}} > FC_{\text{ly}} \tag{A.3}$$

and computed using a storage routing method:

$$w_{\text{perc,ly}} = SW_{\text{ly,excess}} \cdot \left(1 - e^{-\frac{\Delta t}{TT_{\text{perc}}}}\right) \tag{A.4}$$

where Δt is the time step and TT_{perc} is a function of saturated conductivity and FC.

Lateral flow is the subsurface water flow in a soil layer and occurs when saturated soil water moves downslope, calculated as:

$$Q_{\text{lat}} = 0.024 \cdot \frac{SW_{\text{ly,excess}} \cdot K_{\text{s}} \cdot slp}{\phi_d \cdot L_{\text{hill}}} \tag{A.5}$$

where Q_{lat} is lateral flow (mm/day), K_s is saturated hydraulic conductivity (mm/h), slp is slope (m/m), ϕ_d is drainable porosity, and L_{hill} is slope length (m).

To delay lateral response from large hillslopes, which is important for low streamflows, a lag function is used:

$$Q_{\text{lat},i} = Q'_{\text{lat}} + Q_{\text{lat,stor},i-1} \cdot \left(1 - e^{-\frac{1}{TT_{\text{lag}}}}\right) \tag{A.6}$$

where $Q_{\text{lat,stor},i-1}$ is stored lateral flow and TT_{lag} is the lateral flow lag time.

Additionally, SWAT simulates the groundwater re-evaporation (referred to in SWAT+ as **revap**) process, where water from the shallow aquifer moves upward into the overlying unsaturated zone. This occurs during dry periods, as water evaporates from the capillary fringe and is replaced by groundwater, or through direct uptake by deep-rooted vegetation. Water movement from the aquifer to the unsaturated zone is driven by evapotranspiration demand and is controlled by land-cover-specific parameters. **Revap** is important in areas where the water table is close to the surface or where vegetation with deep roots is present, and it is permitted only when the shallow aquifer storage exceeds a threshold defined by the user (aqshthr,rvp).

Other relevant processes influencing soil water dynamics in SWAT include **redistribution** of water between soil layers when moisture exceeds field capacity, evapotranspiration dependent on soil water content available for plants and vegetation leaf area index (LAI), surface runoff calculated with the Curve Number method, and canopy storage, which represents the interception of precipitation by vegetation, temporarily reducing infiltration and enhancing evaporation.

Appendix B

Low Flow Duration is defined as a continuous period during which the daily streamflows, Q_t, are less than $0.2 \cdot \overline{Q}$, where $\overline{Q}$ represents the mean daily streamflows. The threshold is determined using the streamflow percentiles between 0.7 and 0.95.

$$low\_Q\_dur = \frac{1}{N}\sum_{i=1}^{N} D_i \tag{A.7}$$

where low_Q_dur is the Low Flow Duration, N is the number of low streamflow events during the analysis period, and D_i is the duration (in days) of the i-th low streamflow event.

Low Flow Frequency Average number of daily low streamflow events per year (yr^{-1}) with a threshold of 0.2 times the mean daily streamflow. The threshold is determined using the streamflows' percentiles between 0.7 and 0.95.

$$low\_Q\_frec = \frac{N}{T} \tag{A.8}$$

where LFF is the Low Flow Frequency, N is the total number of low streamflow events during the analysis period, and T is the total duration of the analysis period in years.

The Baseflow Index (BFI) is the ratio of baseflow to total streamflow over a specified period (Sawicz et al., 2011; Addor et al., 2018; Westerberg and McMillan, 2015). High values of BFI are observed in catchments with a high baseflow contribution, where water moves through a long streamflow path.

$$BFI = \sum \frac{Q_{\text{B}}}{Q} \tag{A.9}$$

where BFI, Q_{B} is the baseflow at a given time step, and Q is the corresponding total streamflows at the same time step. To calculate BFI, we use the following related equations:

$$Q_{\text{Dt}} = cQ_{\text{Dt-1}} + \frac{1+c}{2}(Q_t - Q_{t-1}) \tag{A.10}$$

where Q_{Dt} is the direct streamflows value at time step t, Q_t is the total streamflows at time step t, and c is a parameter. The value of the baseflow, Q_{Bt}, at time-step t is then given by Equation (5).

$$Q_{\text{Bt}} = Q_t - Q_{\text{Dt}} \tag{A.11}$$

QnDaysMin refers to the mean magnitude of streamflow during the week (7 consecutive days) with the lowest streamflow in the time series (Richter et al., 1996). This can be used to characterize low streamflow segments over a short period, such as during droughts or baseflow conditions.

$$QnDaysMin = \frac{1}{7}\sum_{i=1}^{7} Q_{\text{min},i} \tag{A.12}$$

where, $QnDaysMin$ represents the mean magnitude of streamflow during the week (7 consecutive days) with the lowest streamflow in the

time series. The term $\frac{1}{7}$ indicates that the streamflow values are averaged over a 7-day period. The summation symbol $\sum_{i=1}^{7}$ is the daily sum of streamflow for 7 consecutive days, and $Q_{\min,i}$ represents the daily streamflow on the i-th day of the identified 7-day period with the lowest total streamflow.

To quantify an index of streamflow variability, the slope of the FDC (FDC_slope) is calculated, where a high slope value indicates a variable streamflow regime, while a low slope value indicates a more damped response (Sawicz et al., 2011; Addor et al., 2018).

$$FDC\_slope = \frac{\ln(Q_{33\ \%}) - \ln(Q_{66\ \%})}{0.66 - 0.33} \tag{A.13}$$

where FDC_slope is the slope of the flow duration curve, $Q_{33\ \%}$ is the streamflow value at the 33rd percentile, and $Q_{66\ \%}$ is the streamflow value at the 66th percentile.

Appendix C

Sensitive analysis results are provided in Figs. A.14 and A.15.

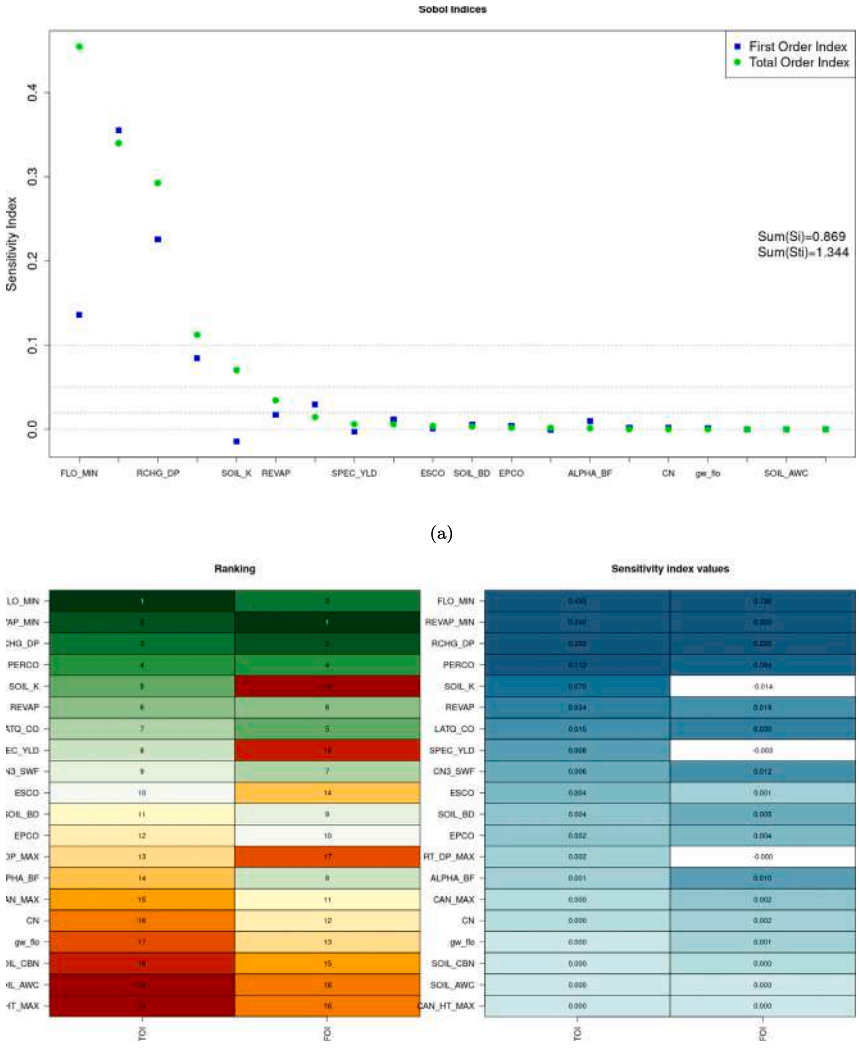

(a) SOBOL analysis index. (b) SOBOL sensitivity rank.

Fig. A.14. (a) SOBOL analysis index. (b) SOBOL sensitivity rank.

Appendix D

Calibrated parameters and their values are provided in Table D.7.

Table D.7
Calibrated parameter values.

N	Parameter	Default value	Range	Change type	Final value CLSoilMapCl	Final value CLSoilMapsTex	Final value HWSDv1.2	Final value DSOLMap
1	FLOW_MIN	3	0–10	replace	9.95	9.28	8.10	8.52
2	REVAP	0.02	0.02–0.2	replace	0.89	0.47	0.66	0.55
3	RCHG_DP	0	0–1	replace	0.32	0.17	0.00	0.21
4	PERCO	0.5	0–1.	replace	0.99	0.77	0.64	0.80
5	REVAP_MIN	5	0–10	replace	2.95	1.30	2.31	0.63
6	LATQ_CO	0.01	0–1	replace	0.34	0.04	0.82	0.21
7	SPEC_YLD	0	0–0.4	replace	0.35	0.15	0.19	0.24
8	CN3_SWF	1	0–1	replace	0.48	0.65	0.98	0.39
9	ESCO	0.5	0.01–1	replace	0.12	0.90	0.01	0.56
10	ALPHA_BF	0.05	0–1	replace	0.20	0.86	0.38	0.67
11	CN2		0.8–1.2	multiplication				

Appendix E

Surface soil water content simulated by various models was compared against station observations, as shown in Fig. A.15.

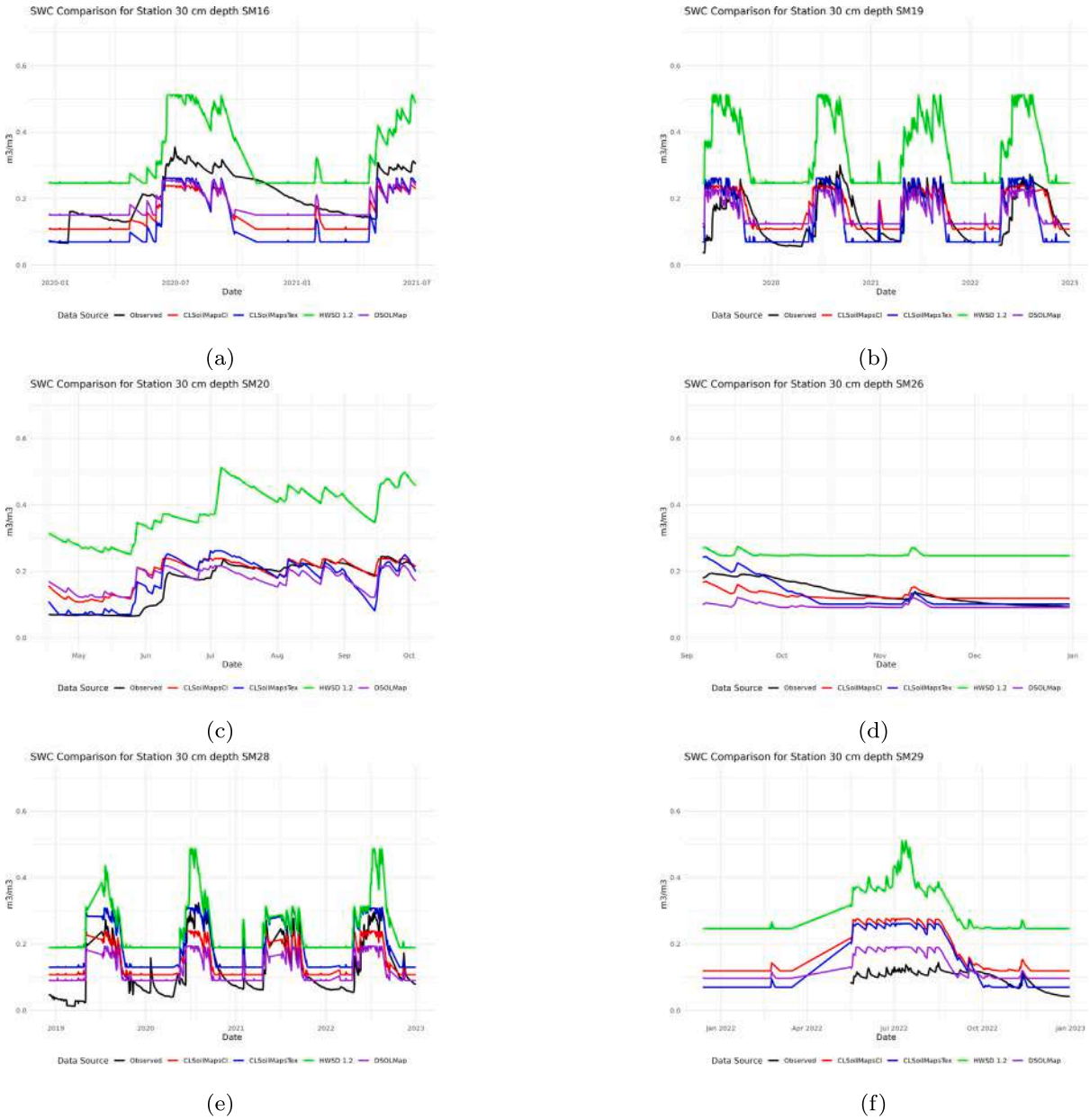

Fig. A.15. Soil Water Content (SWC) at a 30 cm depth. Panel a shows a comparison at the SM16 station. Panel b shows comparison at SM19 station. Panel c shows comparison at SM20 station. Panel d shows comparison at SM26 station. Panel e shows comparison at SM28 station. Panel f shows comparison at SM29 station.

Data availability

Data will be made available on request.

References

Abbaspor, K.C., Vaghefi, S.A., Yang, H., Srinivasan, R., 2019. Global soil, landuse, evapotranspiration, historical and future weather databases for swat applications. Nature, Sci. Data. https://doi.org/10.1038/s41597-019-0282-4

Abitew, T.A., Arnold, J., Jeong, J., Jones, A., Srinivasan, R., 2023. Innovative approach to prognostic plant growth modeling in swat+ for forest and perennial vegetation in tropical and sub-tropical climates. J. Hydrol. X 20, 100156. https://doi.org/10.1016/j.hydroa.2023.100156. https://linkinghub.elsevier.com/retrieve/pii/S2589915523000093.

Addor, N., Nearing, G., Prieto, C., Newman, A.J., Le Vine, N., Clark, M.P., 2018. A ranking of hydrological signatures based on their predictability in space. Water Resour. Res. 54, 8792–8812. https://doi.org/10.1029/2018WR022606. https://agupubs.onlinelibrary.wiley.com/doi/10.1029/2018WR022606.

Arnold, J.G., Moriasi, D.N., Gassman, P.W., Abbaspour, K.C., White, M.J., Srinivasan, R., Santhi, C., Harmel, R.D., van Griensven, A., Van Liew, M.W., Kannan, N., Jha, M.K., 2012. SWAT: model use, calibration, and validation. Trans. ASABE 55, 1491–1508.

Arrouays, D., Richer-de-Forges, A.C., McBratney, A.B., Hartemink, A.E., Minasny, B., Savin, I., Grundy, M., Leenaars, J.G.B., Poggio, L., Roudier, P., Libohova, Z., McKenzie, N.J., Van Den Bosch, H., Kempen, B., Mulder, V.L., Lacoste, M., Chen, S., Saby, N.P.A., Martin, M.P., Román Dobarco, M., Cousin, I., Loiseau, T., Lehmann, S., Caubet, M., Lemercier, B., Walter, C., Vaudour, E., Gomez, C., Martelet, G., Krasilnikov, P., Lagacherie, P., 2018. The Globalsoilmap Project: past, present, future, and national examples from France. Dokuchaev Soil Bull. 3–23. https://doi.org/10.19047/0136-1694-2018-95-3-23.

Bauer, D.F., 1972. Constructing confidence sets using rank statistics. J. Am. Stat. Assoc. 67, 687–690. https://doi.org/10.1080/01621459.1972.10481279. http://www.tandfonline.com/doi/abs/10.1080/01621459.1972.10481279.

Bekele, E.G., Nicklow, J.W., 2007. Multi-objective automatic calibration of swat using NSGA-II. J. Hydrol. 341, 165–176. https://doi.org/10.1016/j.jhydrol.2007.05.014. https://linkinghub.elsevier.com/retrieve/pii/S0022169407002673.

Bieger, K., Arnold, J.G., Rathjens, H., White, M.J., Bosch, D.D., Allen, P.M., Volk, M., Srinivasan, R., 2017. Introduction to SWAT+, a completely restructured version of the soil and water assessment tool. J. Am. Water Resour. Assoc. 53, 115–130. https://doi.org/10.1111/1752-1688.12482

Blum, A.G., Archfield, S.A., Hirsch, R.M., Vogel, R.M., Kiang, J.E., Dudley, R.W., 2019. Updating estimates of low-streamflow statistics to account for possible trends. Hydrol. Sci. J. 64, 1404–1414. https://doi.org/10.1080/02626667.2019.1655148. https://www.tandfonline.com/doi/full/10.1080/02626667.2019.1655148.

Bodenstein, D., Clarke, C., Watson, A., Miller, J., Van Der Westhuizen, S., Rozanov, A., 2022. Evaluation of global and continental scale soil maps for southern Africa using selected soil properties. CATENA 216, 106381. https://doi.org/10.1016/j.catena.2022.106381. https://linkinghub.elsevier.com/retrieve/pii/S0341816222003678.

Boisier, J.P., 2023. CR2MET: a high-resolution precipitation and temperature dataset for the period 1960-2021 in continental Chile (v2.5). Zenodo [Data set]. https://doi.org/10.5281/zenodo.7529682

Boluwade, A., Madramootoo, C., 2013. Modeling the impacts of spatial heterogeneity in the Castor watershed on runoff, sediment, and phosphorus loss using SWAT: i. Impacts of spatial variability of soil properties. Water Air Soil Pollut. 224, 1–16. https://doi.org/10.1007/s11270-013-1692-0

Bouma, J., 2014. Soil science contributions towards sustainable development goals and their implementation: linking soil functions with ecosystem services. J. Plant Nutr. Soil Sci. 177, 111–120. https://doi.org/10.1002/jpln.201300646

Brighenti, T.M., Bonumá, N.B., Grison, F., Mota, A.D.A., Kobiyama, M., Chaffe, P.L.B., 2019. Two calibration methods for modeling streamflow and suspended sediment with the swat model. Ecol. Eng. 127, 103–113. https://doi.org/10.1016/j.ecoleng.2018.11.007. https://linkinghub.elsevier.com/retrieve/pii/S092585741830418X.

Cenobio-Cruz, O., Quintana-Seguí, P., Barella-Ortiz, A., Zabaleta, A., Garrote, L., Clavera-Gispert, R., Habets, F., Beguería, S., 2023. Improvement of low flows simulation in the Saser hydrological modeling chain. J. Hydrol. X 18, 100147. https://doi.org/10.1016/j.hydroa.2022.100147. https://linkinghub.elsevier.com/retrieve/pii/S2589915522000293.

Chagas, V.B.P., Chaffe, P.L.B., Blöschl, G., 2024. Regional low flow hydrology: model development and evaluation. Water Resour. Res. 60, e2023WR035063. https://doi.org/10.1029/2023WR035063. https://agupubs.onlinelibrary.wiley.com/doi/10.1029/2023WR035063.

Chen, F., Crow, W.T., Starks, P.J., Moriasi, D.N., 2011. Improving hydrologic predictions of a catchment model via assimilation of surface soil moisture. Adv. Water Resour. 34, 526–536. https://doi.org/10.1016/j.advwatres.2011.01.011. https://linkinghub.elsevier.com/retrieve/pii/S030917081100025X.

Chen, L., Wang, G., Zhong, Y., Shen, Z., 2016. Evaluating the impacts of soil data on hydrological and nonpoint source pollution prediction. Sci. Total Environ. 563-564, 19–28. https://doi.org/10.1016/j.scitotenv.2016.04.107. http://dx.doi.org/10.1016/j.scitotenv.2016.04.107.

Choudhary, R., Athira, P., 2021. Effect of root zone soil moisture on the swat model simulation of surface and subsurface hydrological fluxes. Environ. Earth Sci. 80, 620. https://doi.org/10.1007/s12665-021-09912-z. https://link.springer.com/10.1007/s12665-021-09912-z.

CIREN, 1997. Estudio agrologico VII región. Erosión de suelos. Descripciones de suelos, materiales y símbolos. CIREN.

CIREN0, 1999. Estudio agrológico VIII región. Descripciones de suelos, materiales y símbolos. Santiago. CIREN.

Cordeiro, M.R.C., Lelyk, G., Kröbel, R., Legesse, G., Faramarzi, M., Masud, M.B., McAllister, T., 2018. Deriving a dataset for agriculturally relevant soils from the Soil Landscapes of Canada (SLC) database for use in soil and water assessment tool (SWAT) simulations. Earth Syst. Sci. Data 10, 1673–1686. https://doi.org/10.5194/essd-10-1673-2018. https://essd.copernicus.org/articles/10/1673/2018/.

Dai, Y., Shangguan, W., Wei, N., Xin, Q., Yuan, H., Zhang, S., Liu, S., Lu, X., Wang, D., Yan, F., 2019. A review of the global soil property maps for EARTH system models. SOIL 5, 137–158. https://doi.org/10.5194/soil-5-137-2019. https://soil.copernicus.org/articles/5/137/2019/.

Dile, Y., Srinivasan, R., George, C., 2015. QGIS interface for SWAT+: (QSWAT+). Setup for Robit Watershed, Lake Tana Basin 1–118. https://doi.org/10.13140/RG.2.1.1060.7201

Dinamarca, D.I., Galleguillos, M., Seguel, O., Faúndez Urbina, C., 2023. CLSoilMaps: a national soil gridded database of physical and hydraulic soil properties for Chile. Sci. Data 10, 630. doi: s41597-023-02536-x.

Entekhabi, D., Njoku, E.G., O'Neill, P.E., Kellogg, K.H., Crow, W.T., Edelstein, W.N., Entin, J.K., Goodman, S.D., Jackson, T.J., Johnson, J., Kimball, J., Piepmeier, J.R., Koster, R.D., Martin, N., McDonald, K.C., Moghaddam, M., Moran, S., Reichle, R., Shi, J.C., Spencer, M.W., Thurman, S.W., Tsang, L., Van Zyl, J., 2010. The soil moisture active passive (SMAP) mission. Proc. IEEE 98, 704–716. https://doi.org/10.1109/JPROC.2010.2043918. http://ieeexplore.ieee.org/document/5460980/.

Fassnacht, F.E., Poblete-Olivares, J., Rivero, L., Lopatin, J., Ceballos-Comisso, A., Galleguillos, M., 2021. Using Sentinel-2 and canopy height models to derive a landscape-level biomass map covering multiple vegetation types. Int. J. Appl. Earth Obs. Geoinf. 94, 102236. https://doi.org/10.1016/j.jag.2020.102236. https://linkinghub.elsevier.com/retrieve/pii/S0303243420308795.

Fernando, S.M., Zhang, L., Feger, K.-H., 2025. Assessing the impact of soil data resolution on streamflow prediction with Swat in a mesoscale headwater basin of Sri Lanka. J. Hydrol. Reg. Stud. 61, 102683. https://doi.org/10.1016/j.ejrh.2025.102683. https://linkinghub.elsevier.com/retrieve/pii/S2214581825005129.

Fischer, G., Nachtergaele, F., Prieler, S., van Velthuizen, H.T., Verelst, L., Wiberg, D. ed), 2008. Harmonized World Soil Database, Version 2.0 ed. Food and Agriculture Organization of the United Nations, Rome.

Galleguillos, M., Ceballos-Comisso, A., Gimeno, F., Zambrano-Bigiarini, M., 2024. Cldynamiclandcover. https://doi.org/10.5281/ZENODO.13153631. https://zenodo.org/doi/10.5281/zenodo.13153631.

Galleguillos, M., Gimeno, F., Puelma, C., Zambrano-Bigiarini, M., Lara, A., Rojas, M., 2021. Disentangling the effect of future land use strategies and climate change on streamflow in a Mediterranean catchment dominated by tree plantations. J. Hydrol. 595, 126047. https://doi.org/10.1016/j.jhydrol.2021.126047

Galleguillos, M., Jacob, F., Prévot, L., Carlos, F., 2017. Estimation of actual evapotranspiration over a rainfed vineyard using a 1-D water transfer model: a case study within a Mediterranean watershed. Agric. Water Manag. 184, 67–76. https://doi.org/10.1016/j.agwat.2017.01.006

Garcia, F., Folton, N., Oudin, L., 2017. Which objective function to calibrate rainfall–runoff models for low-flow index simulations? Hydrol. Sci. J. 62, 1149–1166. https://doi.org/10.1080/02626667.2017.1308511. https://www.tandfonline.com/doi/full/10.1080/02626667.2017.1308511.

Garreaud, R., Boisier, J.P., Álvarez-Garreton, C., Christie, D., Carrasco-Escaff, T., Vergara, I., Chávez, R.O., Aldunce, P., Camus, P., Suazo-Álvarez, M., Masiokas, M., Castro, G., Muñoz, A., Zambrano-Bigiarini, M., Fuster, R., Godoy, L., 2025. Hyperdroughts in central Chile: drivers, impacts and projections. EGUsphere 2025, 1–31. https://doi.org/10.5194/egusphere-2025-517. https://egusphere.copernicus.org/preprints/2025/egusphere-2025-517/.

Gimeno, F., Galleguillos, M., Dinamarca, D., Zambrano-Bigiarini, M., 2024. CLSoilSwat. https://doi.org/10.5281/ZENODO.13933451. https://zenodo.org/doi/10.5281/zenodo.13933451.

Gimeno, F., Galleguillos, M., Manuschevich, D., Zambrano-Bigiarini, M., 2022. A coupled modeling approach to assess the effect of forest policies in water provision: a biophysical evaluation of a drought-prone rural catchment in south-central Chile. Sci. Total Environ. 830, 154608. https://doi.org/10.1016/j.scitotenv.2022.154608. https://linkinghub.elsevier.com/retrieve/pii/S0048969722017016.

González–Zamora, Á., Benito–Verdugo, P., Martínez–Fernández, J., 2024. On the variability in the temporal stability pattern of soil moisture under Mediterranean conditions. Span. J. Soil Sci. 14, 12839. https://doi.org/10.3389/sjss.2024.12839. https://www.frontierspartnerships.org/articles/10.3389/sjss.2024.12839/full.

Gupta, H.V., Kling, H., Yilmaz, K.K., Martinez, G.F., 2009. Decomposition of the mean squared error and Nse performance criteria: implications for improving hydrological modelling. J. Hydrol. 377, 80–91. https://doi.org/10.1016/j.jhydrol.2009.08.003. https://linkinghub.elsevier.com/retrieve/pii/S0022169409004843.

Han, E., Merwade, V., Heathman, G.C., 2012. Implementation of surface soil moisture data assimilation with watershed scale distributed hydrological model. J. Hydrol. 416–417, 98–117. https://doi.org/10.1016/j.jhydrol.2011.11.039. https://linkinghub.elsevier.com/retrieve/pii/S0022169411008249.

Hargreaves, G.H., Samani, Z.A., 1985. Reference crop evapotranspiration from temperature. Appl. Eng. Agric. 1, 96–99. https://doi.org/10.13031/2013.26773

Harrison, R.L., Van Tol, J., Toucher, M.L., 2022. Using hydropedological characteristics to improve modelling accuracy in afromontane catchments. J. Hydrol. Reg. Stud. 39, 100986. https://doi.org/10.1016/j.ejrh.2021.100986. https://linkinghub.elsevier.com/retrieve/pii/S2214581821002159.

Hassan Hayatu, I., Mohammed, A., Ahmad Isma'eel, B., Yusuf Ali, S., 2020. K-means clustering aalgorithm based classification of soil fertility in north west Nigeria. FUDMA J. Sci. 4, 780–787. https://doi.org/10.33003/fjs-2020-0402-363. http://68.169.56.45:80/index.php/fjs/article/view/363.

He, Y., Mao, H., Wang, C., Hu, J., Ninsawat, S., Song, X., Jing, G., Li, R., Wang, M., Duan, Z., 2025. Advancing hydrological modeling through

multivariate calibration of multi-layer soil moisture dynamics. J. Hydrol. Reg. Stud. 57, 102125. https://doi.org/10.1016/j.ejrh.2024.102125. https://linkinghub.elsevier.com/retrieve/pii/S2214581824004749.
Hot, E., Popovic-Bugarin, V., 2016. Soil data clustering by using k-means and fuzzy k-means algorithm. Tel. J. 8, 56–61. https://doi.org/10.5937/telfor1601056H. http://scindeks.ceon.rs/Article.aspx?artid=1821-32511601056H.
Hrachowitz, M., Fovet, O., Ruiz, L., Euser, T., Gharari, S., Nijzink, R., Freer, J., Savenije, H.H.G., Gascuel-Odoux, C., 2014. Process consistency in models: the importance of system signatures, expert knowledge, and process complexity. Water Resour. Res. 50, 7445–7469. https://doi.org/10.1002/2014WR015484. https://agupubs.onlinelibrary.wiley.com/doi/10.1002/2014WR015484.
Hrachowitz, M., Stockinger, M., Coenders-Gerrits, M., Van Der Ent, R., Bogena, H., Lücke, A., Stumpp, C., 2021. Reduction of vegetation-accessible water storage capacity after deforestation affects catchment travel time distributions and increases young water fractions in a headwater catchment. Hydrol. Earth Syst. Sci. 25, 4887–4915. https://doi.org/10.5194/hess-25-4887-2021
Hörmann, G., Köplin, N., Cai, Q., Fohrer, N., 2009. Using a simple model as a tool to parameterise the Swat model of the Xiangxi River in China. Quat. Int. 208, 116–120. https://doi.org/10.1016/j.quaint.2008.11.007. https://linkinghub.elsevier.com/retrieve/pii/S1040618208003364.
Jaffrés, J.B.D., Cuff, B., Cuff, C., Faichney, I., Knott, M., Rasmussen, C., 2021. Hydrological characteristics of Australia: relationship between surface flow, climate and intrinsic catchment properties. J. Hydrol. 603, 126911. https://doi.org/10.1016/j.jhydrol.2021.126911
JAXA, 2007. L1.5_palsar. https://doi.org/10.5067/NXY378J3DFZQ
Kincheon, S.J., 1959. Flow-duration curves. https://doi.org/10.3133/wsp1542A
Kirkby, M.J., 2016. Water in the critical zone: soil, water and life from profile to planet. SOIL 2, 631–645. https://doi.org/10.5194/soil-2-631-2016
Lei, Q., Zhang, T., An, M., Luo, J., Qin, L., Zhu, A.-X., Qiu, W., Du, X., Liu, H., 2024. Sensitivity analysis of swat streamflow and water quality to the uncertainty in soil properties generated by the Solim model. J. Hydrol. 642, 131879. https://doi.org/10.1016/j.jhydrol.2024.131879. https://linkinghub.elsevier.com/retrieve/pii/S0022169424012757.
Li, H., Robock, A., Liu, S., Mo, X., Viterbo, P., 2005. Evaluation of reanalysis soil moisture simulations using updated Chinese soil moisture observations. J. Hydrometeorol. 6, 180–193. https://doi.org/10.1175/JHM416.1. http://journals.ametsoc.org/doi/10.1175/JHM416.1.
Liu, E., Zhu, Y., Calvet, J.-C., Lü, H., Bonan, B., Zheng, J., Gou, Q., Wang, X., Ding, Z., Xu, H., et al., 2024. Evaluation of root zone soil moisture products over the Huai River basin. Hydrol. Earth Syst. Sci. 28, 2375–2400. https://doi.org/10.5194/hess-28-2375-2024,2024
Lopez-Ballesteros, A., Nielsen, A., Castellanos-Osorio, G., Trolle, D., Senent-Aparicio, J., 2023. Dsolmap, a novel high-resolution global digital soil property map for the SWAT + model: development and hydrological evaluation. Catena 231, 107339. https://doi.org/10.1016/j.catena.2023.107339
Martínez–Fernández, J., Molina–Navarro, E., González–Zamora, Á., Sánchez-Gómez, A., Almendra–Martín, L., 2023. Swat soil moisture assessment under Mediterranean conditions: an intercomparison analysis in the Henares basin (Spain). J. Hydrol. Reg. Stud. 48, 101460. https://doi.org/10.1016/j.ejrh.2023.101460. https://linkinghub.elsevier.com/retrieve/pii/S2214581823001477.
McMillan, H., 2020. Linking hydrologic signatures to hydrologic processes: a review. Hydrol. Process. 34, 1393–1409. https://doi.org/10.1002/hyp.13632
Muñoz-Castro, E., Anderson, B.J., Astagneau, P.C., Swain, D.L., Mendoza, P.A., Brunner, M.I., 2025. How well do hydrological models simulate streamflow extremes and drought-to-flood transitions? EGUsphere [preprint]. https://doi.org/10.5194/egusphere-2025-781
Neitsch, S., Arnold, J., Kiniry, J., 2005. Herramienta de evaluación de suelo y agua documentación teórica. Agric. Res. Serv. 415.
Neitsch, S.L., Arnold, J.G., Kiniry, J.R., Williams, J.R., 2011. Soil and Water Assessment Tool Theoretical Documentation Version 2009 Technical Report.
Pandey, A., Bishal, K.C., Kalura, P., Chowdary, V.M., Jha, C.S., Cerdà, A., 2021. A soil water assessment tool (swat) modeling approach to prioritize soil conservation management in river basin critical areas coupled with future climate scenario analysis. Air. Soil Water Res. 14, 11786221211021396. https://doi.org/10.1177/11786221211021395. https://journals.sagepub.com/doi/10.1177/11786221211021395.
Park, G.A., Park, J.Y., Joh, H.K., Lee, J.W., Ahn, S.R., Kim, S.J., 2014. Evaluation of mixed forest evapotranspiration and soil moisture using measured and swat simulated results in a hillslope watershed. KSCE J. Civ. Eng. 18, 315–322. https://doi.org/10.1007/s12205-014-0193-z. https://linkinghub.elsevier.com/retrieve/pii/S122679882403006X.
Pfannerstill, M., Guse, B., Fohrer, N., 2014. Smart low flow signature metrics for an improved overall performance evaluation of hydrological models. J. Hydrol. 510, 447–458. https://doi.org/10.1016/j.jhydrol.2013.12.044. https://linkinghub.elsevier.com/retrieve/pii/S0022169413009414.
Pizarro, A., Jorquera, J., 2024. Advancing objective functions in hydrological modelling: integrating knowable moments for improved simulation accuracy. J. Hydrol. 634, 131071. https://doi.org/10.1016/j.jhydrol.2024.131071. https://linkinghub.elsevier.com/retrieve/pii/S0022169424004669.
Poggio, L., de Sousa, L.M., Batjes, N.H., Heuvelink, G.B.M., Kempen, B., Ribeiro, E., Rossiter, D., 2021. Soilgrids 2.0: producing soil information for the globe with quantified spatial uncertainty. SOIL 7, 217–240. https://doi.org/10.5194/soil-7-217-2021. https://soil.copernicus.org/articles/7/217/2021/.
Pokhrel, P., Yilmaz, K.K., Gupta, H.V., 2012. Multiple-criteria calibration of a distributed watershed model using spatial regularization and response signatures. J. Hydrol. 418–419, 49–60. https://doi.org/10.1016/j.jhydrol.2008.12.004. https://linkinghub.elsevier.com/retrieve/pii/S0022169408005970.
R Core Team, 2025. R: a language and environment for statistical computing. R Foundation for Statistical Computing. Vienna, Austria. https://www.R-project.org/.
Richter, B.D., Baumgartner, J.V., Powell, J., Braun, D.P., 1996. A method for assessing hydrologic alteration within ecosystems. Conserv. Biol. 10, 1163–1174. https://www.jstor.org/stable/2387152.
Rivas-Tabares, D., de Miguel, N., Willaarts, B., Tarquis, A.M., 2020. Self-organizing map of soil properties in the context of hydrological modeling. Appl. Math. Model. 88, 175–189. https://doi.org/10.1016/j.apm.2020.06.044
Rivas-Tabares, D., Tarquis, A.M., Willaarts, B., de Miguel, Á., 2019. An accurate evaluation of water availability in sub-arid Mediterranean watersheds through SWAT: Cega-Eresma-Adaja. Agric. Water Manage. 212, 211–225. https://doi.org/10.1016/j.agwat.2018.09.012. https://linkinghub.elsevier.com/retrieve/pii/S0378377418313672.
Rivera, D., Sandoval, M., Godoy, A., 2015. Exploring soil databases: a self-organizing map approach. Soil Use Manag. 31, 121–131. https://doi.org/10.1111/sum.12169. https://bsssjournals.onlinelibrary.wiley.com/doi/10.1111/sum.12169.
Rubel, F., Kottek, M., 2010. Observed and projected climate shifts 1901-2100 depicted by world maps of the köppen-Geiger climate classification. Meteorol. Z. 19, 135–141. https://doi.org/10.1127/0941-2948/2010/0430
Saltelli, A., Annoni, P., Azzini, I., Campolongo, F., Ratto, M., Tarantola, S., 2010. Variance based sensitivity analysis of model output. Design and estimator for the total sensitivity index. Comput. Phys. Commun. 181, 259–270. https://doi.org/10.1016/j.cpc.2009.09.018. https://linkinghub.elsevier.com/retrieve/pii/S0010465509003087.
Sawicz, K., Wagener, T., Sivapalan, M., Troch, P.A., Carrillo, G., 2011. Catchment classification: empirical analysis of hydrologic similarity based on catchment function in the eastern USA. Hydrol. Earth Syst. Sci. 15, 2895–2911. https://doi.org/10.5194/hess-15-2895-2011. https://hess.copernicus.org/articles/15/2895/2011/.
Schaap, M.G., Leij, F.J., Van Genuchten, M.T., 2001. Rosetta: a computer program for estimating soil hydraulic parameters with hierarchical pedotransfer functions. J. Hydrol. 251, 163–176. https://doi.org/10.1016/S0022-1694(01)00466-8
Seguel, O., Galleguillos, M., Dinamarca, D., Pfeiffer, M., Pérez-Quezada, J., Zambrano-Bigiarini, M., Zamorano, C., Fustos, I., 2023. CHSPD Chilean soil profile database V1. https://doi.org/10.5281/ZENODO.7846566. https://zenodo.org/record/7846566.
Seguel, O., Galleguillos, M., Dinamarca, D., Pfeiffer, M., Pérez-Quezada, J., Zambrano-Bigiarini, M., Zamorano, C., Fustos, I., Casanova, G., 2024. CHSPD Chilean soil profile database V2. https://doi.org/10.5281/ZENODO.13870760. https://zenodo.org/doi/10.5281/zenodo.13870760.
Smakhtin, V.U., 2001. Low flow hydrology: a review. J. Hydrol. 240, 147–186. https://doi.org/10.1016/S0022-1694(00)00340-1. https://linkinghub.elsevier.com/retrieve/pii/S0022169400003401.
Smit, E., Van Zijl, G., Riddell, E., Van Tol, J., 2024a. Examining the value of hydropedological information on hydrological modeling at different scales in the Sabie catchment, South Africa. Vadose Zone J. 23, e20280. https://doi.org/10.1002/vzj2.20280. https://acsess.onlinelibrary.wiley.com/doi/10.1002/vzj2.20280.
Smit, E., Van Zijl, G., Riddell, E., Van Tol, J., 2024b. Model calibration using hydropedological insights to improve the simulation of internal hydrological processes using swat +. Hydrol. Process. 38, e15158. https://doi.org/10.1002/hyp.15158. https://onlinelibrary.wiley.com/doi/10.1002/hyp.15158.
Sobol, I.M., 2001. Global sensitivity indices for nonlinear mathematical models and their monte carlo estimates. Math. Comput. Simul. 55, 271–280. https://doi.org/10.1016/S0378-4754(00)00270-6. https://linkinghub.elsevier.com/retrieve/pii/S0378475400002706.
Soto, L., Galleguillos, M., Seguel, O., Sotomayor, B., Lara, A., 2019. Assessment of soil physical properties' statuses under different land covers within a landscape dominated by exotic industrial tree plantations in south-central Chile. J. Soil Water Conserv. 74, 12–23. https://doi.org/10.2489/jswc.74.1.12. https://www.tandfonline.com/doi/full/10.2489/jswc.74.1.12.
Tegegne, G., Kim, Y.-O., Seo, S.B., Kim, Y., 2019. Hydrological modelling uncertainty analysis for different flow quantiles: a case study in two hydro-geographically different watersheds. Hydrol. Sci. J. 64, 473–489. https://doi.org/10.1080/02626667.2019.1587562. https://www.tandfonline.com/doi/full/10.1080/02626667.2019.1587562.
Tibshirani, R., Walther, G., Hastie, T., 2001. Estimating the number of clusters in a data set via the gap statistic. J. R. Stat. Soc. Ser. B Stat. Methodol. 63, 411–423. https://doi.org/10.1111/1467-9868.00293. https://academic.oup.com/jrsssb/article/63/2/411/7083348.
Van Genuchten, M.T., Leij, F.J., Yates, S.R., 1991. The RETC CODE for Quantifying the Hydraulic Functions of Unsaturated Soils. Technical Report U.S. Environmental Protection Agency, Washington, D.C., EPA/600/2-91/065 (NTIS 92-119668).
Van Tol, J., Bieger, K., Arnold, J.G., 2021. A hydropedological approach to simulate streamflow and soil water contents with swat +. Hydrol. Process. 35, e14242. https://doi.org/10.1002/hyp.14242. https://onlinelibrary.wiley.com/doi/10.1002/hyp.14242.
Van Tol, J.J., Le Roux, P.A.L., Lorentz, S.A., Hensley, M., 2013. Hydropedological classification of South African hillslopes. Vadose Zone J. 12, https://doi.org/10.2136/vzj2013.01.0007
Vanderhoof, M.K., Nieuwlandt, P., Golden, H.E., Lane, C.R., Christensen, J.R., Keenan, W., Dolan, W., 2024. Surface water storage influences streamflow signatures. Hydrol. Earth Syst. Sci. Discuss. https://doi.org/10.5194/hess-2024-119
Vereecken, H., Huisman, J.A., Pachepsky, Y., Montzka, C., van der Kruk, J., Bogena, H., Weihermüller, L., Herbst, M., Martinez, G., Vanderborght, J., 2014. On the spatio-temporal dynamics of soil moisture at the field scale. J. Hydrol. 516, 76–96. https://doi.org/10.1016/j.jhydrol.2013.11.061
Vereecken, H., Weihermüller, L., Assouline, S., Šimůnek, J., Verhoef, A., Herbst, M., Archer, N., Mohanty, B., Montzka, C., Vanderborght, J., Balsamo, G., Bechtold, M., Boone, A., Chadburn, S., Cuntz, M., Decharme, B., Ducharne, A., Ek, M., Garrigues, S., Goergen, K., Ingwersen, J., Kollet, S., Lawrence, D.M., Li, Q., Or, D., Swenson, S.,

de Vrese, P., Walko, R., Wu, Y., Xue, Y., 2019. Infiltration from the pedon to global grid scales: an overview and outlook for land surface modeling. Vadose Zone J. 18, 180191. https://doi.org/10.2136/vzj2018.10.0191

Wang, Z., Sun, S., Wang, G., Song, C., 2023. Determination of low-flow components in alpine permafrost rivers. J. Hydrol. 617, 128886. https://doi.org/10.1016/j.jhydrol.2022.128886. https://linkinghub.elsevier.com/retrieve/pii/S0022169422014561.

Westerberg, I.K., McMillan, H.K., 2015. Uncertainty in hydrological signatures. Hydrol. Earth Syst. Sci. 19, 3951–3968. https://doi.org/10.5194/hess-19-3951-2015. https://hess.copernicus.org/articles/19/3951/2015/.

Williamson, G., 2016. Environmental change Biology tools: ecbtools. https://rdrr.io/github/ozjimbob/ecbtools/.

Yang, Q., Zhang, X., 2016. Improving swat for simulating water and carbon fluxes of forest ecosystems. Sci. Total Environ. 569–570, 1478–1488. https://doi.org/10.1016/j.scitotenv.2016.06.238. https://linkinghub.elsevier.com/retrieve/pii/S0048969716314279.

Yen, H., Ahmadi, M., White, M.J., Wang, X., Arnold, J.G., 2014. C-swat: the soil and water assessment tool with consolidated input files in alleviating computational burden of recursive simulations. Comput. Geosci. 72, 221–232. https://doi.org/10.1016/j.cageo.2014.07.017. https://linkinghub.elsevier.com/retrieve/pii/S0098300414001836.

Yilmaz, K.K., Gupta, H.V., Wagener, T., 2008. A process-based diagnostic approach to model evaluation: application to the Nws distributed hydrologic model. Water Resour. Res. 44, 2007WR006716. https://doi.org/10.1029/2007WR006716. https://agupubs.onlinelibrary.wiley.com/doi/10.1029/2007WR006716.

Zambrano-Bigiarini, M., Clerc, M., Rojas, R., 2013. Standard particle swarm optimisation 2011 at CEC-2013: a baseline for future PSO improvements. In: 2013 IEEE Congress on Evolutionary Computation, CEC 2013 2337–2344. https://doi.org/10.1109/CEC.2013.6557848

Zare, M., Azam, S., Sauchyn, D., 2022. Evaluation of soil water content using swat for southern Saskatchewan, Canada. Water 14, 249. https://doi.org/10.3390/w14020249. https://www.mdpi.com/2073-4441/14/2/249.

Zeraatpisheh, M., Ayoubi, S., Brungard, C.W., Finke, P., 2019. Disaggregating and updating a legacy soil map using Dsmart, fuzzy c-means and k-means clustering algorithms in central Iran. Geoderma 340, 249–258. https://doi.org/10.1016/j.geoderma.2019.01.005. https://linkinghub.elsevier.com/retrieve/pii/S0016706118316197.